



HAL
open science

Dual Solution-/Solid-State Emissive Excited-State Intramolecular Proton Transfer (ESIPT) Dyes: A Combined Experimental and Theoretical Approach

Thibault Pariat, Timothée Stoerkler, Clément Diguët, Adèle Laurent, Denis Jacquemin, Gilles Ulrich, Julien Massue

► **To cite this version:**

Thibault Pariat, Timothée Stoerkler, Clément Diguët, Adèle Laurent, Denis Jacquemin, et al.. Dual Solution-/Solid-State Emissive Excited-State Intramolecular Proton Transfer (ESIPT) Dyes: A Combined Experimental and Theoretical Approach. *Journal of Organic Chemistry*, 2021, 86 (24), pp.17606-17619. 10.1021/acs.joc.1c01698 . hal-03853101

HAL Id: hal-03853101

<https://cnrs.hal.science/hal-03853101>

Submitted on 22 Nov 2022

HAL is a multi-disciplinary open access archive for the deposit and dissemination of scientific research documents, whether they are published or not. The documents may come from teaching and research institutions in France or abroad, or from public or private research centers.

L'archive ouverte pluridisciplinaire **HAL**, est destinée au dépôt et à la diffusion de documents scientifiques de niveau recherche, publiés ou non, émanant des établissements d'enseignement et de recherche français ou étrangers, des laboratoires publics ou privés.

Dual Solution/Solid-State Emissive Excited-State Intramolecular Proton Transfer (ESIPT) Dyes: A Combined Experimental and Theoretical Approach

Thibault Pariat,^{†‡} Timothée Stoerkler,^{†‡} Clément Diguët,[‡] Adèle D. Laurent,^{*‡} Denis Jacquemin,^{*‡} Gilles Ulrich^{*†} and Julien Massue^{*†}

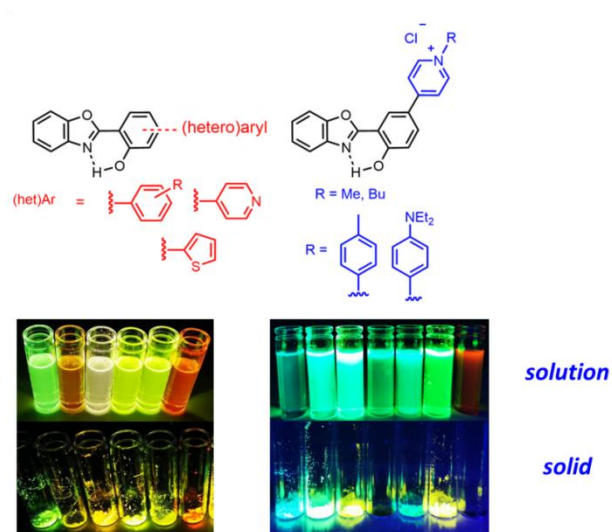
[‡] These authors contributed equally to the work

[†] Institut de Chimie et Procédés pour l'Energie, l'Environnement et la Santé (ICPEES), Equipe Chimie Organique pour la Biologie, les Matériaux et l'Optique (COMBO), UMR CNRS 7515, Ecole Européenne de Chimie, Polymères et Matériaux (ECPM), Université de Strasbourg, 25 Rue Becquerel, 67087 Strasbourg Cedex 02, France

[‡] Laboratoire CEISAM UMR UN-CNRS 6230, Université de Nantes, Nantes F-44000, France

Email: Adele.Laurent@univ-nantes.fr, Denis.Jacquemin@univ-nantes.fr, gulrich@unistra.fr, massue@unistra.fr

Abstract



Excited-State Intramolecular Proton Transfer (ESIPT) dyes typically display strong solid-state emission but faint fluorescence intensity is observed in solution, owing to detrimental molecular motions. This article investigates the influence of the direct (hetero)arylation on the optical properties of 2-(2'-hydroxyphenyl)benzoxazole ESIPT emitters. The synthesis of two series of ESIPT emitters bearing substituted neutral or charged aryl, thiophene, or pyridine rings is reported herein along with full photophysical studies in solution and solid-state, demonstrating dual solution/solid-state emission behavior. Depending on the nature of substitution, several excited-state dynamics are observed: quantitative or partially frustrated ESIPT process or deprotonation of the excited species. Protonation studies revealed that pyridine substitution triggered a strong increase of the quantum yield in solution for the protonated species owing to favorable quinoidal stabilization. These attractive features led to the development of a second series of dyes with alkyl or aryl pyridinium moieties displaying strong tunable solution/solid fluorescence intensity. For each series, *ab initio* calculations helped rationalize and ascertain their behavior in the excited state and the nature of the emission observed by the experimental results.

Introduction

The search for optimized multifunctional fluorescent molecules has fueled extensive fundamental research, owing to their strategic position at the crossroad of many fields of applications, *e.g.*, optoelectronics, biology, and materials. Stimuli-responsive molecular structures with expedite syntheses and improved photophysical properties constantly emerge in the literature, enriching the field of heterocyclic chemistry and providing additional examples of smart molecular fluorophores.¹ In this context, fluorescent dyes displaying Excited-State Intramolecular Proton Transfer (ESIPT) emission appear particularly attractive. ESIPT fluorescence is observed in aromatic cores presenting a 5- or 6-membered H-bonded ring in the ground state and relies on a photoinduced tautomerization between the excited normal (N^*) and tautomeric species (T^*), corresponding in the majority of cases to phenol (E^*) and keto (K^*). Many beneficial characteristics arise from this specific excited-state dynamic, *i.e.*, large Stokes shifts, enhanced photostability, strong solid-state emission and environment-sensitive optical properties, owing to an easily perturbed proton transfer.² Over the years, a large structural variety of ESIPT emitters, including 2-(2'-hydroxyphenyl)benzazoles (HBX),³ triazolo[1,5-a]pyrimidines⁴ or amino-benzoquinolines⁵ among many others⁶ have been reported. Synthetic efforts and rationalization have provided optimized ESIPT dyes which have shown additional topical properties such as reversible mechanochromism⁷ or aggregation-induced emission (AIE).⁸ Several ESIPT fluorophores have been also applied to ratiometric sensing,⁹ white-light emission¹⁰ or anti-counterfeiting.¹¹ A common drawback to ESIPT emitters is, however the weak emission intensity in dilute solution due to the occurrence of molecular motions leading to strong non-radiative deactivations, mainly stemming from accessible conical intersections and twisted intramolecular charge transfers (TICT) occurring after ESIPT. Dual-state emitters (DSSE) have been recently reported and correspond to dyes displaying fluorescence emission in solution but also in the solid-state.¹² These dyes have shown great interest since they can act as solution- and solid-state emitters and therefore target a wider range of applications. To use ESIPT dyes as DSSE fluorophores, one need to increase the solution photoluminescent quantum yield (PLQY) while keeping strong emission in the solid-state. Enhancing molecular rigidity of the π -conjugated cores of ESIPT dyes is likely the key to increase PLQY in the solution state. Indeed, recent examples based on rigidified scaffolds derived from imidazo[1,2-f]phenanthridine,¹³ 2-(2'-hydroxyphenyl)benzimidazoles,¹⁴ and others¹⁵ have showed very promising dual solution/solid-state emission (DSSE). A tenuous balance between quasi-planarity, rigidity and

solubility is necessary to engineer ESIPT-based DSSE compounds. On our part, we have showed that the incorporation of ethynyl-extended aryl or silyl substituents at the periphery of the H-bond donor (phenol ring) of HBX dyes is a facile and straightforward method to increase the corresponding PLQY and the overall brightness (Figure 1a).¹⁶ A marked increase of the luminescence intensity in both apolar and polar media was observed as compared to unsubstituted references. These optimized fluorophores have notably showed interesting random lasing properties in doped polymers.¹⁷ Despite the beneficial rigidification induced by the ethynyl-extended functionalization of the HBX core, the formation of an undesired benzofuran side-product can be observed when the H-donating hydroxy group is ortho substituted.¹⁸ This issue prompted us to find alternative ways to rigidify the HBX skeleton so as to increase the PLQY values in solution. Direct arylation of the HBX core appeared as an attractive and straightforward way to engineer DSSE dyes displaying ESIPT.

In this article, we report on our synthetic efforts by incorporating mono- or bis-aryl (meta or para-substituted phenyl) or heteroaryl (thiophene or pyridine) substituents on the phenol side of 2-(2'-hydroxyphenyl)benzoxazoles (HBO) derivatives (Figure 1b). Photophysical investigations on this first series of dyes prompted us to synthesize additional HBO-pyridine derivatives through an optimized Suzuki-Miyaura cross-coupling reaction. Alkylation or arylation of the latter dyes led to HBO-pyridinium dyes displaying an intense and tunable emission in solution (Figure 1c).

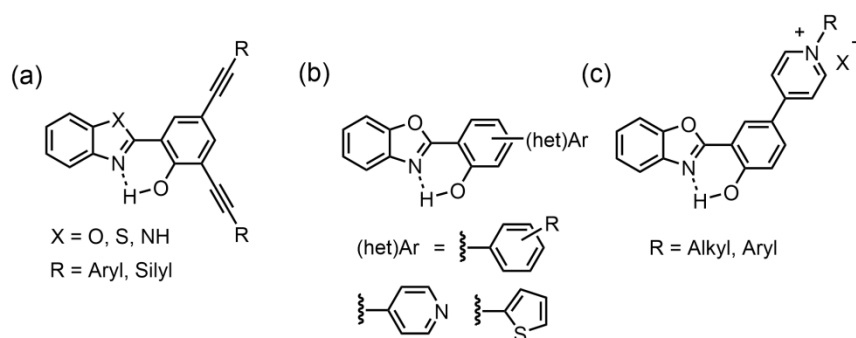


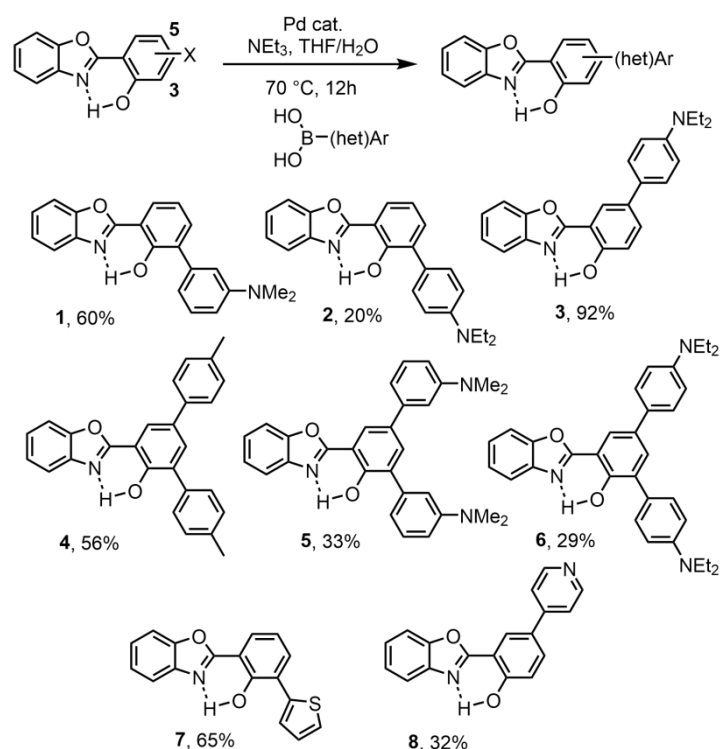
Figure 1. (a) Ethynyl-extended HBX derivatives,^{13b,16-18} (b) (Hetero)arylated HBO dyes (first series) and (c) Alkyl/aryl pyridinium HBO dyes (second series) reported in this article.

Results and Discussion

First Series

Synthesis

The preparation of mono- or bis-substituted dyes **1-8** is described in Scheme 1. Dyes **1-8** were obtained in one step from reported mono-bromo or bis-iodo dyes¹⁶ using a Pd-catalyzed Suzuki-Miyaura cross-coupling reaction with Pd(PPh₃)₂Cl₂ or Pd(dppf)Cl₂ as catalyst. Compounds **1-8** were obtained as yellow powders in 20-92% yield, after purification on column chromatography. It is worth noting that ortho-substituted dyes **2** and **6** were only obtained in 20% and 29% yield respectively, highlighting difficulties to perform cross-coupling at position 3 of the phenol ring with strong donors. All new compounds were characterized by ¹H and ¹³C NMR spectroscopy, as well as HR-MS spectrometry (see the SI).



Scheme 1. Synthesis of (hetero)arylated dyes **1-8**.

Photophysical properties

The photophysical properties of **1-8** are compiled in Table 1 (toluene, dichloromethane, solid) and Table S1 (ethanol). The absorption and emission spectra for **1-8** in toluene are presented on Figure 2 while those recorded in ethanol and dichloromethane can be found on Figures S71 and S72, respectively.

Dyes **1** and **5** functionalized by *m*-N,N-dimethylaniline rings at positions 3 and 3,5 respectively display similar absorption profiles, *i.e.*, broad bands with a maximum absorption wavelength from 329 to 343 nm and molar extinction coefficients ranging between 11500 and

18000 M⁻¹.cm⁻¹. A bathochromic shift of the absorption wavelength is observed for dyes **2,3** and **6** which are functionalized by *p*-N,N,-diethylaniline groups ($\lambda_{\text{abs}} = 352\text{-}392$ nm, $\epsilon = 2600\text{-}18000$ M⁻¹.cm⁻¹, depending on solvent and position of substitution). For dye **4**, exhibiting a bis-tolyl substitution, maximum absorption wavelengths spanning 352-354 nm ($\epsilon = 11200\text{-}11300$ M⁻¹.cm⁻¹) are recorded. In a similar fashion, dyes **7** and **8**, functionalized with heteroaryl rings (thiophene and pyridine) display alike absorption characteristics ($\lambda_{\text{abs}} = 327\text{-}346$ nm, $\epsilon = 12000\text{-}15100$ M⁻¹.cm⁻¹).

Table 1. Photophysical data for dyes **1-8** recorded in aerated solutions at 25°C.

| Dye | Solvent | $\lambda_{\text{abs}}^{[a]}$ (nm) | $\epsilon^{[b]}$ (M ⁻¹ .cm ⁻¹) | λ_{em} (nm) | $\Phi_f^{[c]}$ | $\Delta_{\text{ss}}^{[d]}$ | τ (ns) | $k_r^{[e]}$ | $k_{\text{nr}}^{[e]}$ |
|----------|---|--------------------------------------|--|-------------------------------|----------------|----------------------------|----------------|-------------|-----------------------|
| 1 | toluene | 332 | 16800 | 544 | 0.10 | 11700 | 1.3 | 0.8 | 6.9 |
| | CH ₂ Cl ₂ | 329 | 18000 | 534 | 0.03 | 11700 | 5.4 | 0.06 | 1.8 |
| | CH ₂ Cl ₂ /H ⁺ | 330 | 18200 | 534 | 0.03 | 11600 | 4.7 | 0.06 | 2.1 |
| | solid ^[f] | 330 | - | 528 | 0.18 | 11400 | - | - | - |
| 2 | toluene | 362 | 9200 | 476/599 | 0.04 | 6700 | 2.4 | 0.2 | 4.0 |
| | CH ₂ Cl ₂ | 356 | 9300 | 505/609 | 0.02 | 8300 | 0.5 | 0.4 | 19.6 |
| | CH ₂ Cl ₂ /H ⁺ | 333 | 17700 | 516 | 0.26 | 10700 | 2.5 | 1.0 | 3.0 |
| | solid ^[f] | 360 | - | 440/557 | 0.26 | 5100 | - | - | - |
| 3 | toluene | 375 | 2800 | 470/565 | 0.05 | 5400 | 1.5 | 0.3 | 6.3 |
| | CH ₂ Cl ₂ | 367 | 3100 | 505/586 | 0.05 | 7400 | 3.0 | 0.2 | 3.2 |
| | CH ₂ Cl ₂ /H ⁺ | 336 | 9400 | 506 | 0.09 | 10000 | 3.0 | 0.3 | 3.0 |
| | solid ^[f] | 370 | - | 557 | 0.18 | 9100 | - | - | - |
| 4 | toluene | 354 | 11300 | 550 | 0.11 | 10100 | 1.4 | 0.8 | 6.4 |
| | CH ₂ Cl ₂ | 352 | 12100 | 547 | 0.09 | 10100 | 1.0 | 0.9 | 9.1 |
| | solid ^[f] | 350 | - | 539 | 0.59 | 10000 | - | - | - |
| 5 | toluene | 335 | 12000 | 556 | 0.13 | 11900 | 1.3 | 1.0 | 6.7 |
| | CH ₂ Cl ₂ | 343 | 12900 | 546 | 0.07 | 10900 | 2.0 | 0.4 | 4.7 |
| | CH ₂ Cl ₂ /H ⁺ | 343 | 13300 | 523 | 0.39 | 10000 | 3,9 | 1.0 | 1.6 |
| | solid ^[f] | 335 | - | 465/551 | 0.18 | 8300 | - | - | - |
| 6 | toluene | 392 | 8400 | 475/603 | 0.03 | 4500 | 3.6 | 0.08 | 2.7 |
| | CH ₂ Cl ₂ | 386 | 9100 | 505/609 | 0.05 | 6100 | 0.8 | 0.6 | 11.9 |
| | CH ₂ Cl ₂ /H ⁺ | 348 | 14700 | 525 | 0.35 | 9700 | 2.6 | 1.4 | 2.5 |
| | solid ^[f] | 390 | - | 467/597 | 0.18 | 4200 | - | - | - |
| 7 | toluene | 346 | 12200 | 567 | 0.11 | 11300 | 1.2 | 0.9 | 7.2 |
| | CH ₂ Cl ₂ | 344 | 14100 | 550 | 0.08 | 10900 | 1.2 | 0.7 | 7.6 |
| | solid ^[f] | 340 | - | 566 | 0.37 | 11700 | - | - | - |
| 8 | toluene | 333 | 13200 | 508 | 0.08 | 10400 | 1.5 | 0.5 | 6.1 |
| | CH ₂ Cl ₂ | 332 | 14200 | 497 | 0.12 | 9700 | 3.4 | 0.4 | 2.6 |
| | CH ₂ Cl ₂ /H ⁺ | 330 | 29300 | 490 | 0.55 | 9900 | 3.5 | 1.6 | 1.3 |
| | CH ₂ Cl ₂ /NEt ₃ | 331 | 14000 | 499 | 0.10 | 10000 | 3.4 | 0.3 | 2.7 |
| | solid ^[f] | 330 | - | 496 | 0.38 | 10100 | - | - | - |

^[a] Maximum absorption wavelength (S₀-S₁ transition) ^[b] Absorption coefficient (related to S₀-S₁ transition) ^[c] Relative quantum yield determined in solution using Rhodamine 6G as a reference ($\lambda_{\text{exc}} = 488$ nm, $\Phi = 0.94$ in ethanol), ^[d] Stokes

shift, $^{[e]}$ k_r (10^8 s^{-1}) and k_{nr} (10^8 s^{-1}) were calculated using: $k_r = \Phi_F/\sigma$, $k_{nr} = (1 - \Phi_F)/\sigma$ where σ is the lifetime, $^{[f]}$ as embedded in KBr pellet, PLQY calculated as absolute in an integration sphere fitted to a spectrofluorimeter.

Photoexcitation in the lowest-energy band (330-390 nm) leads to an intense emission in the visible in toluene and dichloromethane but also in ethanol for selected cases (Figures 2, S71 and S72).

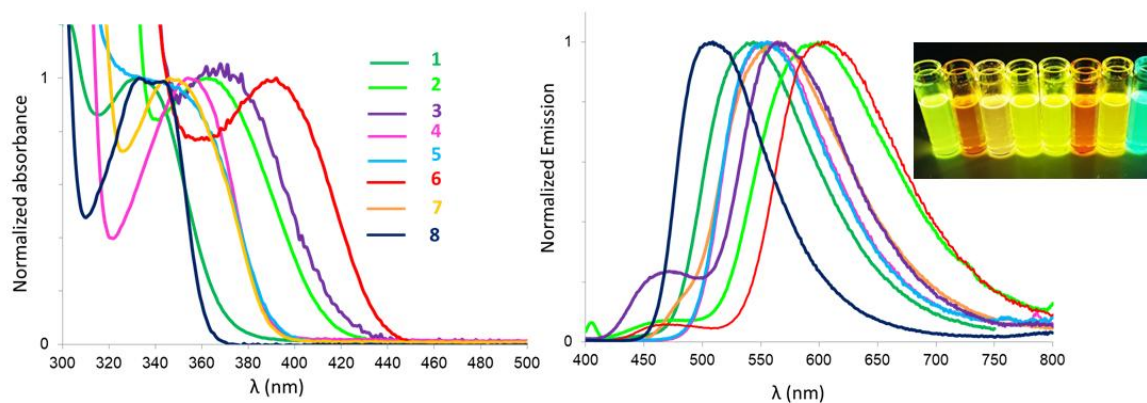


Figure 2. (left) Normalized absorption and (right) Normalized emission spectra of **1** (green), **2** (light green), **3** (purple), **4** (pink), **5** (blue), **6** (red), **7** (orange), and **8** (navy blue) in toluene at 25°C. (Insert) Photographs of solutions of dyes **1-8** in toluene under irradiation from a bench UV-lamp ($\lambda_{exc} = 365 \text{ nm}$).

In toluene, for dyes **1** and **5**, functionalized by a *m*-N,N-dimethylaniline moiety, a single emission band is observed at 544 and 556 nm, attributed to the radiative transition of the K^* tautomer, indicating a quantitative ESIP process in these cases. However, for dyes **2,3** and **6**, the substitution by *p*-N,N-diethylaniline (NEt_2) groups leads to a dual E^*/K^* emission at 476/599, 470/565 and 475/603 nm, respectively. These observations indicate that the electrodonating character of NEt_2 group contributes to the stabilization of the energy level of E^* , leading to a partial frustration of the proton transfer, which is a typical feature in such systems.^{3c,10a,18} It is a clear indication that electron donors tend to decrease the acidity of the phenolic proton in the excited-state (*i.e.* decrease of pKa^*), leading to dual emission. Also, it is worth noting that this dual emission is observed in apolar toluene, highlighting the fact that ESIP frustration is exclusively due to electronic parameters and not solvation effect in protic environment. Also, the position of the NEt_2 functionalization seems to significantly influence the emission wavelength of the resulting dyes when one compare dyes **2** and **3** ($\lambda_{em} = 599$ and 565 nm, respectively). Introduction of the electrodonating moiety at position 3, as in **2** leads to a redshifted emission, evidencing a stronger ICT process than for position 3. A

double NEt_2 functionalization at positions 3 and 5, as in dye **6** does not strongly modify the emission wavelength as compared to a single 5-substitution ($\lambda_{\text{em}} = 599$ and 603 nm for dyes **3** and **6**, respectively). All dyes bearing a N,N-dialkylamino functionalization do not display any fluorescence emission in ethanol. However, dye **4**, substituted by tolyl groups, does display single emission bands both in toluene and ethanol ($\lambda_{\text{em}} = 544$ and 550 nm, respectively). Similarly, in toluene, dyes **7** and **8** present a single K^* emission band whose maximum emission wavelength spans from 508 to 567 nm. Dye **7**, bearing an electrodonating thiophene ring is the most red-shifted one, in part due to a planarization effect, limited in **8** (see theory below). In ethanol, the emission wavelengths for these dyes are similar to those observed in toluene ($\lambda_{\text{em}} = 492$ - 561 nm, Figure S71). The PLQY values recorded in toluene are in the range 3-13% for dyes **1-8**, with the highest values measured for derivatives **1**, **4**, and **5** incorporating a double aryl functionalization with a tolyl or *m*-N,N,-dimethylaniline groups. Dyes **2**, **3**, and **6** with peripheral NEt_2 moieties are the least fluorescent ones, providing a further evidence of the presence of detrimental ICT processes in these dyes. These PLQY are overall higher than those observed for unsubstituted HBO dyes,^{16a} highlighting the beneficial role of the peripheral aryl or heteroaryl groups but are significantly lower than those induced by the ethynyl-extended moieties previously reported.^{16,17} For the entire series of dyes bearing N,N,-dialkylaniline groups, the fluorescence emission appears to be completely quenched in ethanol. The fluorescence lifetimes are all in the nanosecond range which is characteristic of organic fluorophores. A monoexponential decay is systematically found, even in the case of a dual E^*/K^* emission.

Solid-state emission

The photophysical properties in the solid-state were recorded as embedded in potassium bromide pellets. The emission spectra of dyes **1-8** in solid are presented on Figure 3.

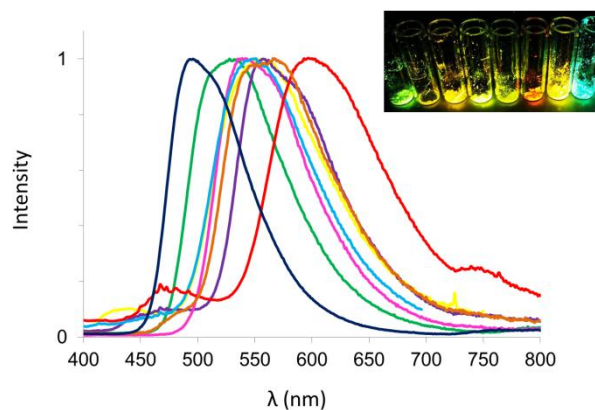


Figure 3. Emission in the solid-state, as embedded in KBr pellets (concentration of around 10^{-4} M) of **1** (green), **2** (yellow), **3** (purple), **4** (pink), **5** (blue), **6** (red), **7** (orange), and **8** (navy blue). (Insert) Photographs of solutions of dyes **1-8** as powders under irradiation from a bench UV-lamp ($\lambda_{\text{exc}} = 365$ nm).

The maximum emission wavelengths are rather similar to those observed in solution, *i.e.*, maxima spanning 496-597 nm. It is to be noted that all dyes display a single K^* band, with the exception of dyes **2**, **3**, **5** and **6** where a dual E^*/K^* emission is observed ($\lambda_{\text{em}}(E^*) = 440-465$ nm), albeit with a relatively weak contribution from the phenol. The PLQY recorded as absolute, with an integration sphere fitted to a spectrophotometer, are in the 18-59% range, which represents a strong increase as compared to those recorded in solution. This feature, a trademark among ESIPT dyes, is attributed to a restriction of molecular motions in the excited-state, and in particular the rotation around the central double bond of the K^* form.

Protonation studies

All dyes featuring a dialkylamino group display optical characteristics attributed to an ICT process (see theory below). In order to shed more light on this process but also on the overall influence of external stimuli on the optical response, the photophysical properties of the dyes carrying protonable groups, *i.e.* dyes **1-3**, **5**, **6**, and **8** were studied in their protonated state, in dichloromethane and ethanol (Tables 1 and S1, Figures 4, S73 and S74).

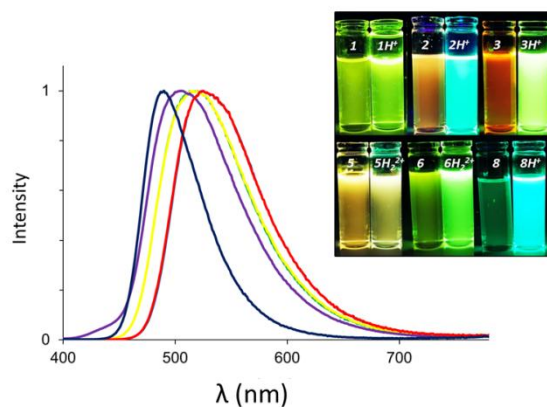


Figure 4. Emission spectra of **1** (green), **2** (yellow), **3** (purple), **5** (blue), **6** (red), **8** (navy blue) in their protonated state in dichloromethane at 25°C. (Insert) Photographs of solution in neutral (left) and protonated (right) dichloromethane under irradiation from a bench UV-lamp ($\lambda_{\text{exc}} = 365 \text{ nm}$).

Protonation of the selected dyes was performed by bubbling HCl gas into a solution of the dyes in dichloromethane or ethanol. As a general trend, for dyes **1** and **5** with a *m*-N,N,-dimethylaniline group, the protonation does not drastically modify the maximum absorption wavelength, whereas a marked blue-shift is observed for those carrying at least one *p*-NEt₂, namely dyes **2**, **3**, and **6** ($\lambda_{\text{abs}} = 356\text{-}386 \text{ nm}$ vs. $333\text{-}348 \text{ nm}$ in dichloromethane in their neutral and protonated state, respectively). This feature is accompanied by an important hyperchromic effect and is also observed in ethanol. Upon photoexcitation in the lowest-energy band, an intense emission band is observed in all cases, whose nature could be attributed to the decay of the K* tautomer. Indeed, protonation of the lone electron pair of the nitrogen tends to decrease the electronic density on the π -conjugated cores of the dyes and further favor the ESIPT process (see theory below). Previous examples showed that protonation triggered a disappearance of dual emission to the benefit of a single band.^{16b} The most striking feature observed in the course of the protonation studies is the significant increase of the PLQY as compared to their neutral counterparts, peaking at 39% for dye **5** in the N,N-dialkylated aniline series. Dye **8**, functionalized with a pyridine at position 5 stands out in the series. Indeed, protonation does not trigger major changes in terms of emission wavelength neither in dichloromethane, nor in ethanol ($\lambda_{\text{em}} = 497$ and $430/492 \text{ nm}$ vs. $\lambda_{\text{em}} = 490$ and 501 nm in their neutral/protonated state, in dichloromethane and ethanol, respectively). The PLQY significantly increases in protonated dichloromethane (55%) but not ethanol which hints at a strong contribution from solvation in this case. We hypothesize that these enhanced optical properties in dichloromethane arise from the formation of a stabilized

quinoidal excited species (Figure 5). In the neutral state, the pyridine moiety favors complete deprotonation of the excited phenol leading to the impossibility of ESIPT to occur and the emission of the resulting phenolate. Indeed, it is reported that phenolate moieties derived from HBO dyes can be highly emissive.^{13b,18b} Moreover, the formation of the phenolate in neutral dichloromethane is consistent with the *ab initio* calculations (see below). To further evidence deprotonation in the excited-state, absorption and emission spectra of dye **8** in presence of 0.1% a base (NEt_3) were recorded, leading to similar maximum wavelengths ($\lambda_{\text{abs}}/\lambda_{\text{em}} = 333/498 \text{ nm}$) as in neutral dichloromethane (Figure S75). Upon protonation of both phenolate and pyridine moieties, ESIPT can occur, which is further stabilized through the formation of a quinoidal exciton by H-bonding (Figure 5). The significant increase of PLQY in the protonated species might stem, not only from H-bonded rigidification but also from the lack of proton-coupled electron transfer (PCET) process, as reported in a related example.²⁰ In ethanol, reported solvation occurs in the ground and excited-state of HBX dyes, thereby inhibiting the subsequent stabilization through the excited quinoidal species (Figure 5).

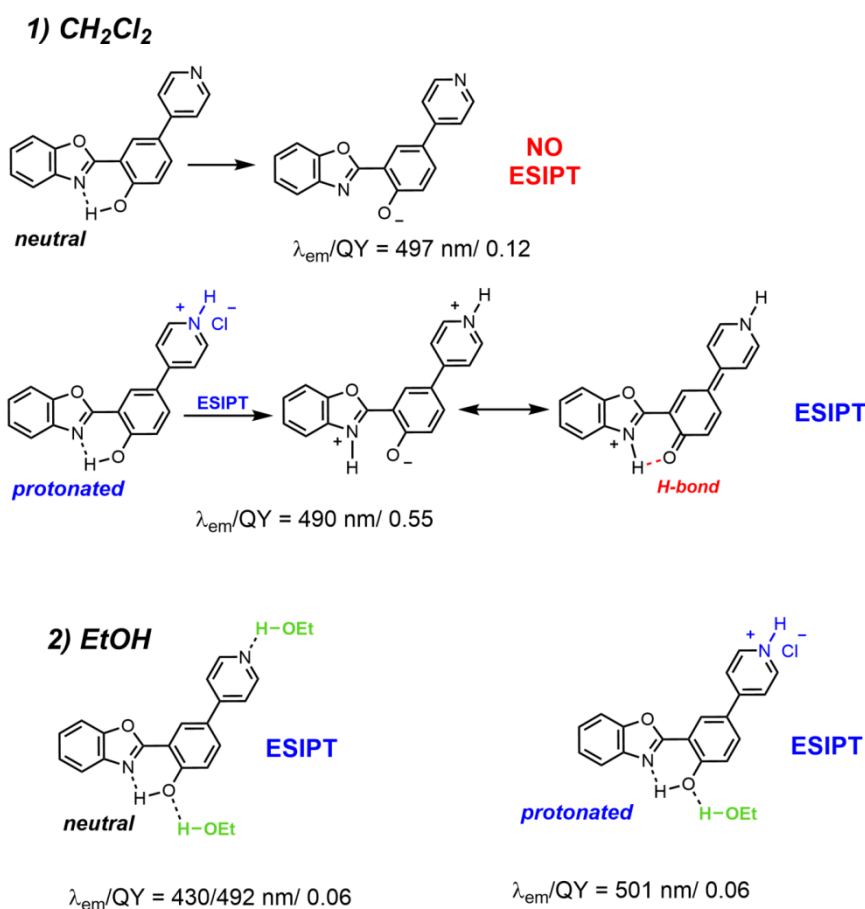


Figure 5 Solvation effects in 1) dichloromethane and in 2) ethanol on the photophysical properties of **8**.

Theoretical modelling

Following our usual strategy,¹⁷⁻¹⁹ first principle calculations were performed in order to complement the experimental characterizations and obtained details regarding the electronic structures of the investigated compounds. First, we checked that only the phenol form is present in the ground electronic state. As can be seen in Table S3 in the SI, the keto isomer is indeed unstable in the ground state (higher than the proton transfer transition state on the free energy scale), and the structures presenting a O \cdots HO H-bonding pattern are also much less stable than their N \cdots HO counterparts. As can be seen in Table S4, the latter conclusion also holds in the excited-state. The main theoretical results related to emission are summarized in Table 2. For all dyes, considering the absorption in toluene, the lowest excited state is always very intense and located on the HBO core. For dyes **1-6**, the most red-shifted absorption is computed for dye **6** ($\lambda_{\text{abs}} = 379$ nm), in good agreement with the experimental measurement ($\lambda_{\text{abs}} = 392$ nm, Figure 2), given the fact that theoretical modelling neglects vibronic couplings and hence logically delivers slightly blue-shifted wavelengths as compared to experiment. This can be explained qualitatively, by the electronic density difference plots displayed in Figure S105; in dye **6**, the two amino groups located *para* participate to the excited-state, whereas this effect is much milder in **5** which presents a *meta*-substitution pattern leading to a more localized excited state, hence appearing at higher energy. For dyes **7** and **8**, theory correctly foresees that **7** possesses the largest absorption wavelength (Figure 2). From Figure S3.1, it is quite obvious that the thienyl ring is actively participating in the excited state as a donor group, owing to its smaller dihedral angle with respect to the HBO core, whereas the direct impact of the pyridyl group present in **8**, that is more twisted, is smaller.

Table 2. Computed vertical absorption and (phenol and keto) vertical emission wavelengths together with the excited state free energy difference between the phenol and keto forms ($\Delta G^{\text{K}^*-\text{E}^*}$) and the phenol and the ESIPT transition state ($\Delta G^{\text{TS}^*-\text{E}^*}$). Negative values for the latter are due to vibrational corrections and are indicative of barrierless transfer. See the Method Section for technical details.

| Dye | Solvent | λ_{abs} (nm) | $\lambda_{\text{em}}(\text{E}^*)$ (nm) | $\lambda_{\text{em}}(\text{K}^*)$ (nm) | $\Delta G^{\text{K}^*-\text{E}^*}$ (eV) | $\Delta G^{\text{TS}^*-\text{E}^*}$ (eV) |
|----------|---|--------------------------------|---|---|--|---|
| 1 | toluene | 327 | 398 | 513 | -0.24 | -0.02 |
| 2 | toluene | 367 | 457 | 577 | -0.16 | 0.00 |
| 2 | CH ₂ Cl ₂ | 367 | 510 | 603 | -0.20 | 0.01 |
| 2 | CH ₂ Cl ₂ /H ⁺ | 312 | 374 | 515 | -0.41 | -0.06 |
| 3 | toluene | 367 | 453 | 550 | -0.07 | 0.04 |

| | | | | | | |
|----------|---|-----|-----|-------------------------|-------|-------|
| 3 | CH ₂ Cl ₂ | 371 | 503 | 584 | -0.12 | 0.04 |
| 3 | CH ₂ Cl ₂ /H ⁺ | 312 | 373 | 495 | -0.28 | 0.03 |
| 4 | toluene | 334 | 396 | 529 | -0.25 | -0.01 |
| 5 | toluene | 338 | 399 | 530 | -0.23 | -0.01 |
| 6 | toluene | 379 | 459 | 590 | -0.15 | 0.00 |
| 7 | toluene | 328 | 397 | 531 | -0.30 | -0.04 |
| 8 | toluene | 314 | 363 | 479 | -0.25 | -0.01 |
| 8 | CH ₂ Cl ₂ | 311 | 373 | 487, 469 ^[a] | -0.29 | 0.00 |
| 8 | CH ₂ Cl ₂ /H ⁺ | 355 | 433 | 528 | -0.24 | 0.06 |

^[a] Anionic form

As for the emission in toluene for the dyes **1-6** series, there is a significant driving force for inducing ESIPT as the keto isomer is always more stable than the phenol, which is consistent with the formation of K* in the excited state (Table 2). However, the relative stabilization of the keto form significantly varies with the substitution pattern. Indeed, in dyes **1**, **4**, and **5**, the K* tautomer is more stable than its E* counterpart by values exceeding -0.20 eV, which is indicative of quantitative proton transfer.¹⁸ Indeed, experimentally, only the emission from the tautomer is observed for these dyes (Figure 2), with emission wavelengths of 544, 550, and 556 nm, for **1**, **4**, and **5**, respectively. Theory foresees slightly blue-shifted fluorescence at 513, 529, and 530 nm, respectively, for the keto structure. In contrast, the emissions computed for the corresponding phenols fall in the 396-399 nm range, *i.e.*, clearly do not fit experiment. This clearly confirms the presence of ESIPT in these systems. In dyes **2** and **6**, the driving force for proton transfer remains large of *ca.* -0.15 eV, and a very small phenol emission can be found experimentally (Figure 2). Again the computed and measured wavelengths are in good agreement. For **3**, the phenol and keto forms in the excited state become closer to isoenergetic ($\Delta G^{E^*-K^*} = -0.07$ eV), there is a non-trilling barrier for the transfer ($\Delta G^{TS^*-E^*} = 0.04$ eV), and consistently the E* emission becomes significantly more intense in the experimental fluorescence spectrum (Figure 2). Indeed, a $\Delta G^{E^*-K^*}$ in between 0.00 and -0.15 eV is typical of dual emitters.¹⁹ Qualitatively, there is indeed a strong ICT from the amino group towards the dye's core in **3** (Figure S105), explaining that the photoacidity of the hydroxyl is smaller than in, *e.g.* dye **5**. In the **7-8** series, the values listed in Table 2 clearly indicate that only ESIPT emission should be observed, consistent with the experiments. One also notes that whilst the absorption of **7** is only slightly red-shifted as compared to the one of dye **8** (*ca.* +12 nm in both theory and experiment), the K* emission is comparatively more displaced (+59 nm experimentally, +52 nm theoretically). This larger Stokes shift in **7** can be explained its planarization in the excited state; the thienyl moiety becomes fully coplanar with the dye core

in the relaxed K^* structure (true C_s minimum). The spectral properties of dyes **2**, **3**, and **8** were also investigated in dichloromethane, considering both the neutral and protonated forms, so as to closely model the experimental protonation experiments. For dyes **2** and **3**, going from toluene to CH_2Cl_2 has little impact on the absorption spectra, but strongly/significantly red-shifts the E^*/K^* emissions. This trend is related to the much larger excited state dipole of the phenol tautomer (17.6 D for E^* of **2**) as compared to its keto counterpart (6.8 D for K^* of dye **2**). Experimentally, there is clearly a stronger overlap between the phenol and keto emission bands of both **2** and **3** in CH_2Cl_2 than in toluene (see the SI). In terms of driving force for ESIPT, the change of solvent has no drastic impact (Table 2). In contrast, when protonating the amine group, one can notice a stronger driving force for ESIPT, consistent with the fact that only K^* fluorescence is observed experimentally. This can be easily explained by looking at the electron density difference plots displayed in Figure 6: when protonating the amine, the donor character of that group is lost and the excited state becomes more localized on the HBO core with a much stronger decrease of the electron density on the hydroxyl group, indicative of stronger photo-acidic character of OH after protonation. In the same time, this more localized excited state is logically significantly blue-shifted as compared to the one of the neutral form, a trend found in both theory and experiment.

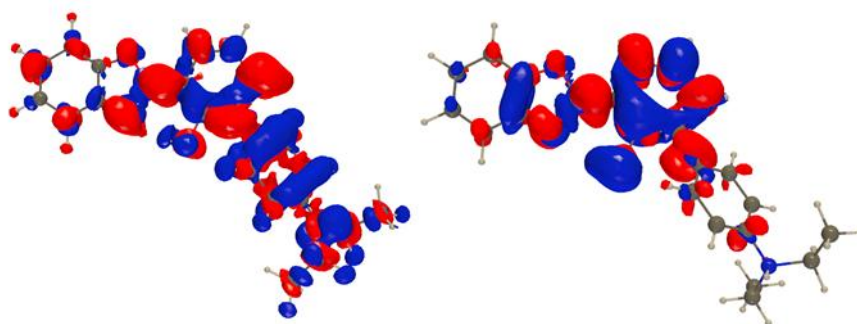


Figure 6. Density difference plots of the lowest excited states of dye **2** (left) and **2.H⁺** in CH_2Cl_2 . Blue and red lobes correspond to decrease and increase of density upon absorption. Contour threshold: 1×10^{-3} au.

For **8** in dichloromethane, theory foresees a strong driving force for ESIPT. However, the predicted emission of K^* (487 nm) is slightly red-shifted as compared to toluene (479 nm), whereas a blue-shift is obtained experimentally (Table 1). As discussed above, this is an indication that the emission of **8** is coming from the anion in dichloromethane, with a computed emission indeed blue-shifted (469 nm) as compared to toluene, qualitatively

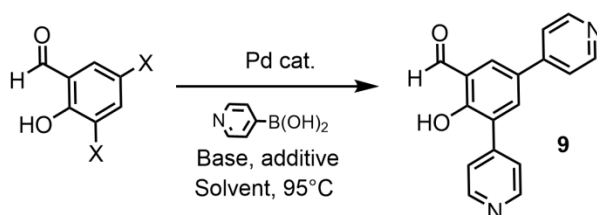
consistent with the measurements. We note however that considering the absolute emission energies would not have allowed attribution, because the difference between the computed emission wavelengths between the two species are within the error bar of our calculation model. For the protonated **8**, theory clearly foresees quantitative ESIPT (driving force of -0.24 eV) with a sole K^* fluorescence at 528 nm, i.e., slightly red-shifted as compared to experiment (490 nm). The geometry of K^* has indeed a quinoidal character as hypothesized above.

Second Series

Synthesis

In order to shed more light on the interesting protonation-responsive photophysical behavior observed for dye **8**, we decided to synthesize ortho-substituted and bis-substituted HBO pyridine derivatives to check if similar properties were observed. Moreover, based on Figure 4, we anticipate that the alkylation or arylation of the pyridine moiety in dye **8** would lead to highly emissive charged fluorophores. Pyridinium derivatives have indeed attracted wide attention due to potential applications from drugs to materials.²¹ Also, pyridinium-²² and benzopyrylium²³-based ESIPT dyes have already shown to induce NIR emission, paving the way to innovative materials for ratiometric sensing. A second series of dyes were therefore developed to further investigate the influence of pyridine/pyridinium moieties on the ESIPT process and the resulting emission intensity in solution and solid-state. Unfortunately, the Suzuki-Miyaura reaction conditions developed on Scheme 1 did not allow any observation of the desired isomer of **8**, nor on 3-bromoHBO, neither on 3,5-dibromoHBO, probably owing to unfavorable electronic interactions at the 3-position of the salicylaldehyde. Optimization of the Pd-catalyzed cross-coupling reaction was then performed on commercially available 3,5-dibromoosalicylaldehyde with variations of the nature of the catalyst, base and solvent (Table 3).

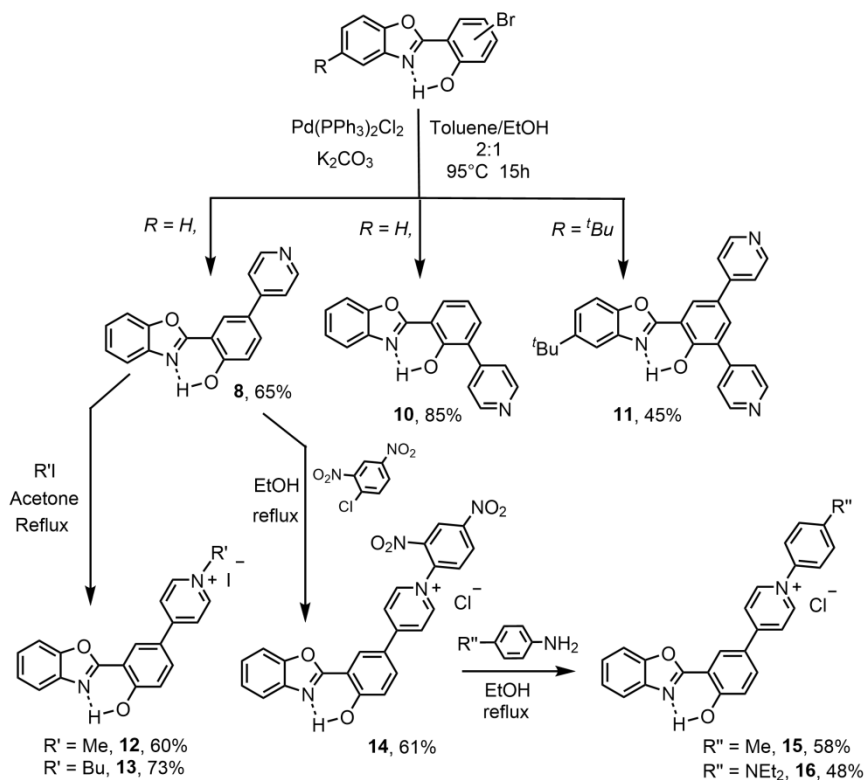
Table 3. Optimization conditions of the Suzuki-Miyaura coupling for the synthesis of salicylaldehyde **9**.



| Entry | X | Pd cat. | Base | Additive | Solvent | Time | Yield |
|-------|----|--|------------------------------------|---------------------|---------------------------------------|------------|-------------|
| 1 | I | PdCl ₂ (PPh ₃) ₂ | NEt ₃ | - | THF/H ₂ O 40:1 | 15h | No reaction |
| 2 | I | PdCl ₂ (PPh ₃) ₂ | K ₂ CO ₃ | - | Dioxane/H ₂ O 4:1 | 15h | No reaction |
| 3 | I | PdCl ₂ (dppf) | K ₂ CO ₃ | LiCl | Dioxane/H ₂ O 4:1 | 39h | No reaction |
| 4 | I | Pd(PPh ₃) ₄ | K ₂ CO ₃ | - | Dioxane/H ₂ O 4:1 | 15h | No reaction |
| 5 | Br | PdCl ₂ (PPh ₃) ₂ | K ₂ CO ₃ | - | Dioxane/H ₂ O 4:1 | 15h | No reaction |
| 6 | Br | PdCl ₂ (dppf) | K ₂ CO ₃ | - | Dioxane/H ₂ O 4:1 | 15h | No reaction |
| 7 | Br | PdCl ₂ (PPh ₃) ₂ | K ₂ CO ₃ | - | Dioxane | 15h | No reaction |
| 8 | Br | PdCl ₂ (PPh ₃) ₂ | CuCO ₃ | - | Dioxane/H ₂ O 4:1 | 15h | No reaction |
| 9 | Br | PdCl ₂ (PPh ₃) ₂ | Ba(OH) ₂ | - | Dioxane/H ₂ O 4:1 | 15h | No reaction |
| 10 | Br | PdCl ₂ (PPh ₃) ₂ | CaCO ₃ | - | Dioxane/H ₂ O 4:1 | 15h | No reaction |
| 11 | Br | PdCl ₂ (PPh ₃) ₂ | CdCO ₃ | - | Dioxane/H ₂ O 4:1 | 15h | No reaction |
| 12 | Br | PdCl ₂ | K ₂ CO ₃ | (O)PPh ₃ | DMF/H ₂ O 2:1 | 15h | No reaction |
| 13 | Br | PdCl₂(PPh₃)₂ | K₂CO₃ | - | Toluene/EtOH 2/1 | 15h | 65% |
| 14 | Br | Pd(PPh ₃) ₄ | K ₂ CO ₃ | - | Toluene/EtOH 2/1 | 15h | 54% |
| 15 | Br | PdCl ₂ (dppf) | K ₂ CO ₃ | - | Toluene/EtOH 2/1 | 15h | 51% |
| 16 | Br | PdCl ₂ (PPh ₃) ₂ | Na ₂ CO ₃ | - | Toluene/EtOH 2/1 | 15h | 22% |
| 17 | Br | PdCl ₂ (PPh ₃) ₂ | Cs ₂ CO ₃ | - | Toluene/EtOH 2/1 | 15h | No reaction |
| 18 | Br | PdCl ₂ (PPh ₃) ₂ | K ₂ CO ₃ | - | Toluene/EtOH 4/1 | 15h | Traces |
| 19 | Br | PdCl ₂ (PPh ₃) ₂ | Cs ₂ CO ₃ | - | Toluene/EtOH 4/1 | 15h | 17% |
| 20 | Br | PdCl ₂ (dppf) | Cs ₂ CO ₃ | - | Toluene/EtOH 1/1 | 15h | No reaction |
| 21 | Br | PdCl ₂ (PPh ₃) ₂ | ^t BuONa | - | Toluene/EtOH 4/1 | 15h | Traces |
| 22 | Br | PdCl ₂ (PPh ₃) ₂ | K ₂ CO ₃ | - | Toluene/EtOH /H ₂ O 12/2/1 | 15h | No reaction |
| 23 | Br | PdCl ₂ (dppf) | K ₂ CO ₃ | - | Toluene/EtOH /H ₂ O 12/2/1 | 15h | No reaction |

During the course of our optimization, we found out that the nature of the solvents is of utmost importance for the cross-coupling to proceed. Presence of water, even in small proportion leads in all cases to the absence of target compound on the crude NMR spectrum. The nature of the inorganic base plays an important role in the success of the coupling, but more surprisingly, the nature of the cation in the carbonate base employed seems to have a strong impact on the reaction yield (K₂CO₃>Na₂CO₃>Cs₂CO₃, see entries 13, 16, 17 in Table 3). Pyridine is a strong chelating moiety, presumably leading to pronounced interactions with cations during the Suzuki coupling. Finally, the nature of the catalyst seems to induce smaller variations of reaction yields (entries 13-15). Eventually, the use of PdCl₂(PPh₃)₂ as 5% mol. catalyst with potassium carbonate as a base in toluene/ethanol (2/1) led to salicylaldehyde **9** in 65% yield, after purification on column chromatography. These optimized reactions

conditions were then applied to 3-bromo, 5-bromo HBO and 3,5-dibromo-*tert*-butyl-HBO dyes to provide dyes **8**, **10-11** in 45-85% yield (Scheme 2).



Scheme 2. Synthesis of dyes **8** and **10-16**.

The optimized cross-coupling conditions led to a strong increase of the synthesis yield of dye **8** (65% vs. 32%) as compared to the conditions developed in Scheme 1 but also provided access to both the isomer **10** and the bis-pyridine derivative **11**. Alkyl pyridinium dyes **12** and **13** were obtained in a straightforward synthesis using a slight excess of methyl or *n*-butyliodide and purified by reprecipitation methods. Arylpyridinium-substituted **15** and **16** were synthesized in two steps, inspired by a Zincke-type reaction protocol.²⁴

Photophysical properties

The photophysical properties of all pyridine/pyridinium containing dyes are presented on Tables 4 and S2 and the emission spectra in solution and solid in Figures 7 and 8, respectively. Photographs of DCM solutions of all dyes in the presence of acid or base can be found on Figure S95.

Table 4. Photophysical data of dyes **10-13** and **15, 16** in dichloromethane at 25°C. The data for dye **8**, taken from Table 1 are reproduced for comparisons

| Dye | Solvent | $\lambda_{\text{abs}}^{[a]}$ (nm) | $\epsilon^{[b]}$ ($\text{M}^{-1}\cdot\text{cm}^{-1}$) | λ_{em} (nm) | $\Phi_{\text{f}}^{[c]}$ | $\Delta_{\text{ss}}^{[d]}$ | τ (ns) | $k_{\text{r}}^{[e]}$ | $k_{\text{nr}}^{[e]}$ |
|-----------|---|--------------------------------------|--|-------------------------------|-------------------------|----------------------------|----------------|----------------------|-----------------------|
| 8 | CH ₂ Cl ₂ | 332 | 14200 | 497 | 0.12 | 9700 | 3.4 | 0.4 | 2.6 |
| 8 | CH ₂ Cl ₂ /H ⁺ | 330 | 29300 | 490 | 0.55 | 9900 | 3.5 | 1.6 | 1.3 |
| 8 | Solid ^[d] | 330 | - | 496 | 0.38 | 10100 | - | - | - |
| 10 | CH ₂ Cl ₂ | 335 | 15900 | 518 | 0.40 | 10500 | 3.1 | 1.29 | 1.94 |
| 10 | CH ₂ Cl ₂ /H ⁺ | 344 | 13500 | 527 | 0.64 | 10100 | 3.6 | 1.78 | 1.00 |
| 10 | Solid ^[d] | 334 | - | 505 | 0.38 | - | - | - | - |
| 11 | CH ₂ Cl ₂ | 347 | 14900 | 520 | 0.58 | 9600 | 4.3 | 1.35 | 0.97 |
| 11 | CH ₂ Cl ₂ /H ⁺ | 341 | 17700 | 511 | 0.56 | 9800 | 4.1 | 1.37 | 1.07 |
| 11 | Solid ^[d] | 345 | - | 541 | 0.22 | - | - | - | - |
| 12 | CH ₂ Cl ₂ | 345 | 22600 | 509 | 0.43 | 9400 | 2.9 | 1.48 | 1.97 |
| 12 | CH ₂ Cl ₂ /H ⁺ | 353 | 23900 | 506 | 0.46 | 8600 | 2.9 | 1.59 | 1.86 |
| 13 | CH ₂ Cl ₂ | 354 | 19300 | 506 | 0.61 | 8500 | 2.9 | 2.10 | 1.34 |
| 13 | CH ₂ Cl ₂ /H ⁺ | 355 | 23700 | 507 | 0.60 | 8400 | 2.9 | 2.07 | 1.38 |
| 13 | Solid ^[d] | 352 | - | 423/511 | 0.08 | - | - | - | - |
| 15 | CH ₂ Cl ₂ | 372 | 21000 | 534 | 0.50 | 8200 | 1.8 | 2.78 | 2.78 |
| 15 | CH ₂ Cl ₂ /H ⁺ | 373 | 21700 | 534 | 0.51 | 8100 | 1.9 | 2.68 | 2.58 |
| 15 | Solid ^[d] | 370 | - | 563 | 0.29 | - | - | - | - |
| 16 | CH ₂ Cl ₂ | 498 | 8000 | 600 | 0.10 | 3400 | 1.3 | 0.77 | 6.92 |
| 16 | CH ₂ Cl ₂ /H ⁺ | 373/470 | 7300 | 526/611 | 0.06 | 2300 | 0.7 | 0.86 | 13.40 |

^[a] Maximum absorption wavelength (S_0 - S_1 transition) ^[b] Absorption coefficient (related to S_0 - S_1 transition) ^[c] Relative quantum yield determined in solution using Rhodamine 6G as a reference ($\lambda_{\text{exc}} = 488$ nm, $\Phi = 0.94$ in ethanol), ^[d] Stokes shift, ^[e] k_{r} (10^8 s^{-1}) and k_{nr} (10^8 s^{-1}) were calculated using: $k_{\text{r}} = \Phi_{\text{f}}/\sigma$, $k_{\text{nr}} = (1 - \Phi_{\text{f}})/\sigma$ where σ is the lifetime, ^[f] as embedded in KBr pellet, PLQY calculated as absolute in an integration sphere fitted to a spectrofluorimeter.

Dyes **10-13** and **15,16** display maximum absorption wavelengths in the UV region ($\lambda_{\text{abs}} = 335$ - 372 nm) which are mildly red-shifted upon formation of the pyridinium moieties, with the exception of **16** where a strong absorption band at 498 nm is observed (Figure S76). This band could be attributed either to a strong charge transfer band from the NEt₂-phenyl group to the pyridinium, or alternatively to the effect of deprotonation leading to the phenolate (see theoretical calculations below).

Photoexcitation in the S_0 - S_1 transition leads to the appearance of an intense emission of light for all dyes, in dichloromethane. **10** which features a pyridine group at the ortho position of the phenol shows red-shifted emission, as compared to its para analogue **8** ($\lambda_{\text{em}} = 518$ vs. 497 nm). The introduction of two pyridine groups, as in **11** leads to very similar emission properties as those of **10** ($\lambda_{\text{em}} = 520$ nm). For those three dyes, a single emission band is

recorded, which we attribute to the formation of the anion, on the basis of spectral comparisons performed after the addition of base (Table S2). Dyes **10** and **11** are very emissive with QY in the range 40-58%, much higher than dyes **1-7** described earlier in dichloromethane. Protonation of these dyes leads to a red-shifted emission in the case of **10** ($\lambda_{em} = 527$ vs. 518 nm) and a blue-shifted emission for **11** ($\lambda_{em} = 520$ vs. 511 nm). The latter is reminiscent to what was observed for **8** and was attributed to an excited quinoidal species (Figure 5).

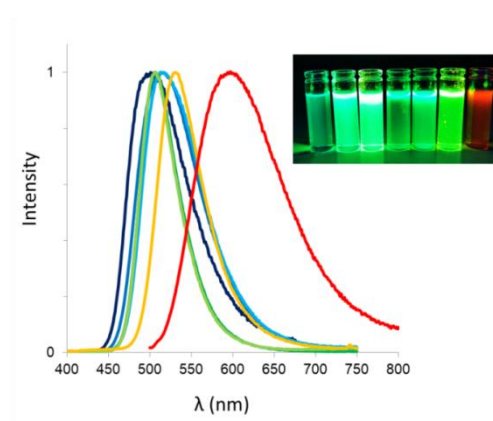


Figure 7. Emission of dye **8** (light blue), **10** (blue), **11** (navy blue), **12** (green), **13** (light green), **15** (orange), and **16** (red) in dichloromethane at 25 °C. (Insert) Photographs of solutions of dyes **8**, **10-13** and **15-16** in dichloromethane under irradiation from a bench UV-lamp ($\lambda_{exc} = 365$ nm).

Formation of alkyl pyridinium dyes **12** and **13** triggered a mild bathochromic emission shift as compared to protonated **8** ($\lambda_{em} = 506$ and 507 vs. 490 nm for **12**, **13** and protonated **8**, respectively). Unlike dyes **8**, **10-11**, the emissions of both **12** and **13** can be attributed to the sole decay of the K^* tautomer, as a result of a quantitative ES IPT process. Indeed, addition of acid does not modify the optical properties ($\lambda_{abs}/\lambda_{em}/QY$), whereas addition of base leads to the appearance of the red-shift band in absorption, consistent with the formation of a zwitterionic pyridinium-phenolate species. The red-shift observed for dyes **12** and **13** vs. protonated **8** is also consistent with a further stabilization of the quinoidal species with the presence of an additional carbon atom. Changing a methyl for a butyl chain as in **13**, does not trigger optical changes in solution, as expected but one can note that **13** is emissive in the solid whereas **12** is not. Introduction of aryl pyridinium moieties, as in dyes **15** and **16** leads to red-shifted emission in both cases, especially in the case of **16** ($\lambda_{em} = 600$ nm). Addition of acid does not modify the emission wavelength in the case of **15** and **16**, highlighting a K^*

emission. In both cases, addition of base leads to the appearance of an intense red-shifted absorption band and a complete quenching of emission (Table S2). It is worth noting that the QY of dye **15** in DCM is reaching 0.50, due to an enhanced stabilization of the excited species via quinoidal delocalization. Calculations return that the ESIPT process is totally frustrated in the case of **16** (see below), presenting a stabilized zwitterionic form in the ground-state. We also note that the Stokes shift in **16** is much smaller than in the other dyes consistent with the absence of ESIPT.

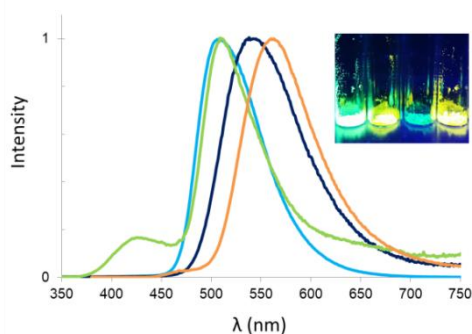


Figure 8. Emission in the solid-state, as embedded in KBr pellets (concentration of around 10^{-4} M) of **10** (blue), **11** (navy blue), **13** (light green), and **15** (orange). (Insert) Photographs of solutions of dyes **10**, **11**, **13** and **15** as powders under irradiation from a bench UV-lamp ($\lambda_{\text{exc}} = 365$ nm).

In the solid-state, only dyes **10**, **11**, **13** and **15** present sizeable emission, with a single or dual emission wavelength spanning 423-563 nm. The QY are significantly lower than those in solution (QY = 0.08-0.38), which is untypical for ESIPT dyes and could be due to enhanced π -stacking or unfavorable electrostatic interactions occurring in the solid-state.

15, functionalized with a tolyl pyridinium moiety appears therefore to be the most promising dye in both series for DSE applications (QY_(DCM) = 0.50, QY_(solid) = 0.29) with a quantitative ESIPT emission.

Theoretical modelling

Similarly to the first series, theoretical calculations were carried out to obtain more insights into the photophysical properties of the second series of dyes (Table 5) and representation of the excited states is available in Figure S106. In the case of dyes **10** and **11**, like for dye **8**, there is a strong driving force for ESIPT, irrespective of the protonation of the pyridyl(s)

groups. Interestingly, in the protonated **11**, it is the group attached at position 3 that acts as the main acceptor, whereas in **15**, it is the donor moiety at position 5 that is mainly involved in the excited state (compare Figures S105 and S106). This difference in electronic flow upon absorption can be understood by the relative weights of the HOMO and LUMO orbitals on these two positions (Figure S107), as donor (acceptor) groups mainly tune the former (latter) orbitals. One can also notice that for the three HBO pyridine isomers **8**, **10** and **11**, the computed emission wavelengths are similar for the anionic and keto species, so that it is *a priori* difficult to perform a definitive attribution on the sole basis of the calculations in that specific case. The pyridinium series **12**, **15** and **16** show very contrasted results (Table 5). For the two former dyes, the K^* tautomer is strongly favored as compared to the phenol, and the keto emissions are computed at 525 nm for **12** and 550 nm for **15**, quite nicely fitting the experimental values of 506 and 534 nm, respectively (Table 4). As can be seen in Figure S106, in both **12** and **15**, the lowest transition corresponds to a strong CT from the HBO core to the pyridinium group, implying a significant decrease of the electron density onto the hydroxyl, consistent with the occurrence of ESIPT. In the case of **12**, we also envisaged the emission from the zwitterionic species (deprotonation yielding the phenolate) but the resulting calculations led to a dark state with both TD-DFT and CC2 level of theory, indicating that such species, if it exists, would not be emissive.

The situation strongly differs in the case of dye **16**. First, for the absorption of the pyridinium species, theory predicts an absorption at 482 nm, in line with the experimental value (498 nm in CH_2Cl_2 , 470 nm in $\text{CH}_2\text{Cl}_2/\text{H}^+$). This strongly red-shifted absorption as compared to the other dyes is explainable by the very strong CT occurring in the system from the *para*- NEt_2 group toward the pyridinium moiety with a negligible change of density onto the hydroxyl (Figure 8). Such CT-like topology prevents the ESIPT process to take place. Indeed, the K^* isomer is computed to be less stable than the E^* (Table 5) in **16**. The computed emission for the E^* is redshifted, similarly to the experiment but the theoretical value seems too large. Taking into consideration the possibility of a deprotonation leading to a phenolate zwitterion, theory returns absorption at 473 nm, very similar to the value determined above for the E^* isomer; although the topology of the excited state between E^* and D^* is totally different (Figure 9). In the case of D^* , a strong CT is taking place between the phenolate and the pyridinium moieties with the amino group being an almost passive element. In summary for dye **16**, the exact nature of the emissive species remains elusive but it is very clear that ESIPT is totally frustrated in this case.

Table 5. Computed vertical absorption and (phenol and keto) vertical emission wavelengths together with the free energy difference between the phenol and keto forms ($\Delta G^{K^*-E^*}$) and the phenol and the ESIPT transition state ($\Delta G^{TS^*-E^*}$). See the Method Section for technical details.

| Dye | Solvent | λ_{abs} (nm) | $\lambda_{em}(E^*)$ (nm) | $\lambda_{em}(K^*)$ (nm) | $\Delta G^{K^*-E^*}$ (eV) | $\Delta G^{TS^*-E^*}$ (eV) |
|-----------|---|-------------------------|-----------------------------|-----------------------------|------------------------------|-------------------------------|
| 8 | CH ₂ Cl ₂ | 311 | 373 | 487/469 ^[a] | -0.29 | 0.00 |
| 8 | CH ₂ Cl ₂ /H ⁺ | 355 | 433 | 528 | -0.24 | 0.06 |
| 10 | CH ₂ Cl ₂ | 312 | 374 | 506/511 ^[a] | -0.39 | -0.04 |
| 10 | CH ₂ Cl ₂ /H ⁺ | 353 | 458 | 478 | -0.42 | -0.04 |
| 11 | CH ₂ Cl ₂ | 323 | 386 | 516/506 ^[a] | -0.41 | -0.04 |
| 11 | CH ₂ Cl ₂ /H ⁺ | 347 | 442 | 540 | -0.51 | -0.05 |
| 12 | CH ₂ Cl ₂ | 353 | 430 | 525 | -0.26 | 0.05 |
| 15 | CH ₂ Cl ₂ | 369 | 459 | 550 | -0.17 | 0.08 |
| 16 | CH ₂ Cl ₂ | 482/473 ^[a] | 702 | 629/543 ^[a] | +0.09 | 0.17 |

^[a] Anionic/zwitterionic form

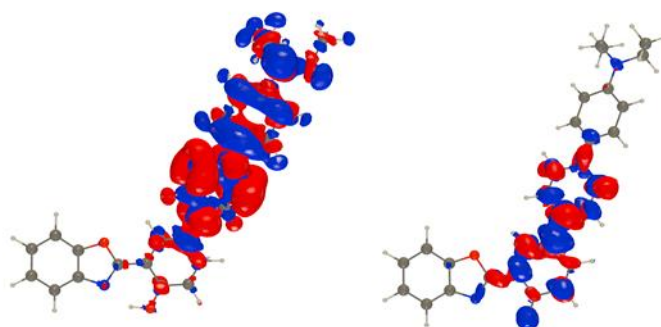


Figure 9. Density difference plots of the lowest excited states of **1-** (left) and **16-H⁺** (phenolate) in CH₂Cl₂. Blue and red lobes correspond to decrease and increase of density upon absorption. Contour threshold: 1×10^{-3} au.

Conclusion

In conclusion, two series of (hetero)arylated HBO dyes have been synthesized and studied and showed intense emission both in solution and/or in the solid-state. Moreover, in the case of pyridine, protonation triggered enhancement of luminescence due to a stabilization of the excited species which prompted the synthesis of a series of alkyl and aryl pyridinium dyes presenting finely tuned emission properties. In this context, *ab initio* calculations appeared as an indispensable tool to provide insightful information on the nature of the excited-state and led to the development of DSSE dyes purely based on ESIPT emission. Due to the strong

environment-responsive features of ESIPT, future developments on these dyes involve probes for biomolecules sensing or bioimaging. Work along these lines is currently in progress.

Experimental section

3-bromo- and 5-bromo-2-(2'-hydroxyphenyl)benzoxazole were obtained from reported procedures.¹⁶

General procedure for the synthesis of dyes 1-3 and 7-8: To a solution of 3-bromo or 5-bromo HBO (1 mmol) in a mixture THF/H₂O (40 mL/1 mL) was added Pd(dppf)Cl₂ (0.2 mmol), triethylamine (10 mmol) and the corresponding boronic acid (3 mmol). The resulting mixture was stirred overnight under reflux using an oil bath. The solution was then taken up in CH₂Cl₂, washed with saturated NH₄Cl solution, dried over MgSO₄ and concentrated *in vacuo*. The crude residue was purified by silica gel chromatography to afford **1-3** and **7-8** as white to orange solids.

1: Purification by flash chromatography eluting with Pet. Ether/ CH₂Cl₂ (6:4). Pale yellow solid (198 mg, 60 %). ¹H NMR (500 MHz, CDCl₃) δ 11.92 (s, 1H), 8.05 (dd, ³J = 7.9 Hz, ⁴J = 1.8 Hz, 1H), 7.75 – 7.70 (m, 1H), 7.66 – 7.61 (m, 1H), 7.55 (dd, ³J = 7.5 Hz, ⁴J = 1.7 Hz, 1H), 7.42 – 7.37 (m, 2H), 7.35 (dd, ³J = 8.3 Hz, 7.5 Hz, 1H), 7.09 (t, ³J = 7.7 Hz, 1H), 7.07 – 7.04 (m, 1H), 7.02 (d, ³J = 7.5 Hz, 1H), 6.82 – 6.77 (m, 1H), 3.02 (s, 6H). ¹³C{¹H} NMR (126 MHz, CDCl₃) δ 163.4, 156.2, 150.7, 149.3, 140.1, 138.5, 134.8, 131.4, 128.9, 126.4, 125.5, 125.1, 119.5, 119.4, 118.1, 114.1, 112.1, 110.9, 110.8, 40.9. HRMS (ESI-TOF) m/z: [M+H] Calcd for C₂₁H₁₉N₂O₂ 331.1441; Found 331.1423.

2: Purification by flash chromatography eluting with Cyclohexane / CH₂Cl₂ (6:4). Pale orange solid (72 mg, 20 %). ¹H NMR (500 MHz, CDCl₃) δ 11.93 (s, 1H), 7.98 (dd, ³J = 7.8 Hz, ⁴J = 1.7 Hz, 1H), 7.75 – 7.69 (m, 1H), 7.65 – 7.60 (m, 1H), 7.60 – 7.55 (m, 2H), 7.52 (dd, ³J = 7.5 Hz, ⁴J = 1.7 Hz, 1H), 7.41 – 7.36 (m, 2H), 7.06 (t, ³J = 7.7 Hz, 1H), 6.82 – 6.75 (m, 2H), 3.42 (q, ³J = 7.1 Hz, 4H), 1.22 (t, ³J = 7.1 Hz, 6H). ¹³C{¹H} NMR (126 MHz, CDCl₃) δ 163.6, 156.2, 149.3, 147.2, 140.2, 134.1, 130.7, 130.4, 125.4, 125.3, 125.1, 124.4, 119.6, 119.4, 111.4, 110.8, 110.8, 44.5, 12.8. HRMS (ESI-TOF) m/z: [M+H] Calcd for C₂₃H₂₃N₂O₂ 359.1754; Found 359.1760.

3: Purification by flash chromatography eluting with Pet. Ether/ CH₂Cl₂ (6:4). Pale yellow solid (330 mg, 92 %). ¹H NMR (500 MHz, CDCl₃) δ 11.39 (s, 1H), 8.20 (d, ⁴J = 2.4 Hz, 1H), 7.81 – 7.71 (m, 1H), 7.68 – 7.59 (m, 2H), 7.57 – 7.47 (m, 2H), 7.42 – 7.34 (m, 2H), 7.16 (d, ³J = 8.6 Hz, 1H), 6.83 – 6.74 (m, 2H), 3.41 (q, ³J = 7.1 Hz, 4H), 1.21 (t, ³J = 7.1 Hz, 6H).

$^{13}\text{C}\{^1\text{H}\}$ NMR (126 MHz, CDCl_3) δ 163.3, 157.3, 149.3, 147.2, 140.3, 133.3, 131.8, 127.6, 127.1, 125.5, 125.1, 124.3, 119.4, 117.8, 112.2, 110.8, 110.7, 44.6, 12.8. HRMS (ESI-TOF) m/z : $[\text{M}+\text{H}]$ Calcd for $\text{C}_{23}\text{H}_{23}\text{N}_2\text{O}_2$ 359.1754; Found 359.1746.

7: Purification by flash chromatography eluting with Cyclohexane / CH_2Cl_2 (9:1). White solid (191 mg, 65 %). ^1H NMR (500 MHz, CDCl_3) δ 12.46 (s, 1H), 8.00 (dd, $^3J = 7.8$ Hz, $^4J = 1.6$ Hz, 1H), 7.82 (dd, $^3J = 7.7$ Hz, $^4J = 1.6$ Hz, 1H), 7.78 – 7.73 (m, 1H), 7.70 (dd, $^4J = 3.7$ Hz, 1.2 Hz, 1H), 7.66 – 7.61 (m, 1H), 7.44 – 7.37 (m, 3H), 7.15 (dd, $^4J = 3.7$ Hz, 1.4 Hz, 1H), 7.07 (t, $^3J = 7.8$ Hz, 1H). $^{13}\text{C}\{^1\text{H}\}$ NMR (126 MHz, CDCl_3) δ 163.1, 155.2, 149.3, 139.9, 138.9, 132.3, 127.3, 126.2, 126.2, 125.8, 125.7, 125.3, 123.3, 119.7, 119.4, 111.4, 110.9. HRMS (ESI-TOF) m/z : $[\text{M}+\text{H}]$ Calcd for $\text{C}_{17}\text{H}_{12}\text{NO}_2\text{S}$: 294.0583; Found 294.0597.

8: Purification by flash chromatography eluting with Pet. Ether/ Ethyl acetate (8:2). Orange solid (92 mg, 32 %). ^1H NMR (500 MHz, CDCl_3) δ 11.70 (s, 1H), 8.69 (d, $^3J = 6.2$ Hz, 2H), 8.34 (d, $^4J = 2.4$ Hz, 1H), 7.88 – 7.71 (m, 2H), 7.71 – 7.63 (m, 1H), 7.61 – 7.53 (m, 2H), 7.48 – 7.39 (m, 2H), 7.24 (d, $^3J = 8.6$ Hz, 1H). $^{13}\text{C}\{^1\text{H}\}$ NMR (126 MHz, CDCl_3) δ 162.4, 159.5, 150.4, 149.2, 147.1, 139.9, 132.0, 129.5, 125.8, 125.5, 125.3, 121.1, 119.5, 118.4, 111.2, 110.8. HRMS (ESI-TOF) m/z : $[\text{M}+\text{H}]$ Calcd for $\text{C}_{18}\text{H}_{12}\text{N}_2\text{O}_2$ 289.0972; Found 289.0981.

General procedure for the synthesis of dyes 4-6: To a solution of 3,5-diiodo HBO (0.45 mmol) in a mixture of toluene/ H_2O (15 mL/1 mL) was added $\text{Pd}(\text{PPh}_3)_2\text{Cl}_2$ (0.13 mmol), diisopropylethylamine (4.5 mmol) and the corresponding boronic acid (2.7 mmol). The resulting mixture was stirred overnight under reflux, using an oil bath. The solution was then taken up in CH_2Cl_2 , washed with saturated NaHCO_3 solution, dried over MgSO_4 and concentrated *in vacuo*. The crude residue was purified by silica gel chromatography to afford dyes **4-6** as white to yellow solids.

4: Purification by flash chromatography eluting with Cyclohexane / CH_2Cl_2 (98:2). White solid (99 mg, 56 %). ^1H NMR (500 MHz, CDCl_3) δ 11.96 (s, 1H), 8.26 (d, $^4J = 2.4$ Hz, 1H), 7.76 – 7.71 (m, 2H), 7.68 – 7.64 (m, 1H), 7.63 – 7.60 (m, 2H), 7.59 – 7.56 (m, 2H), 7.43 – 7.38 (m, 2H), 7.33 – 7.27 (m, 4H), 2.44 (s, 3H), 2.42 (s, 3H). $^{13}\text{C}\{^1\text{H}\}$ NMR (126 MHz, CDCl_3) δ 163.3, 155.4, 149.4, 140.1, 137.4, 137.3, 137.1, 134.8, 133.3, 132.8, 130.8, 129.8, 129.5, 129.1, 126.7, 125.6, 125.2, 124.3, 119.5, 111.2, 110.8, 21.4, 21.3. HRMS (ESI-TOF) m/z : $[\text{M}+\text{H}]$ Calcd for $\text{C}_{27}\text{H}_{22}\text{NO}_2$ 392.1645; Found 392.1659.

5: Purification by flash chromatography eluting with Pet. Ether / CH_2Cl_2 / Ethyl Acetate (70:28:2). Yellow solid (67 mg, 33 %). ^1H NMR (500 MHz, CDCl_3) δ 11.93 (s, 1H), 8.27 (d, $^4J = 2.4$ Hz, 1H), 7.80 (d, $^4J = 2.4$ Hz, 1H), 7.77 – 7.71 (m, 1H), 7.68 – 7.63 (m, 1H), 7.43 – 7.32 (m, 4H), 7.09 – 7.06 (m, 2H), 7.06 – 7.01 (m, 1H), 7.01 – 6.96 (m, 1H), 6.81 (dd, $^3J =$

8.4 Hz, $^4J = 2.6$ Hz, 1H), 6.77 (dd, $^3J = 8.2$ Hz, $^4J = 2.6$ Hz, 1H), 3.03 (s, 6H), 3.01 (s, 6H). $^{13}\text{C}\{^1\text{H}\}$ NMR (126 MHz, CDCl_3) δ 163.4, 155.6, 151.2, 150.7, 149.4, 141.3, 140.2, 138.6, 133.9, 133.8, 131.6, 129.7, 129.0, 125.6, 125.2, 124.8, 119.4, 118.2, 115.6, 114.1, 112.1, 111.7, 111.3, 111.0, 110.9, 40.9. HRMS (ESI-TOF) m/z : $[\text{M}+\text{H}]$ Calcd for $\text{C}_{29}\text{H}_{28}\text{N}_3\text{O}_2$: 450.2176; Found 450.2198.

6: Purification by flash chromatography eluting with Cyclohexane / Ethyl Acetate (95:5). Yellow solid (66 mg, 29 %). ^1H NMR (500 MHz, CDCl_3) δ 11.86 (s, 1H), 8.16 (d, $^4J = 2.4$ Hz, 1H), 7.78 – 7.69 (m, 2H), 7.68 – 7.60 (m, 3H), 7.60 – 7.51 (m, 2H), 7.45 – 7.34 (m, 2H), 6.88 – 6.74 (m, 4H), 3.44 (q, $^3J = 6.9$ Hz, 4H), 3.43 (q, $^3J = 6.9$ Hz, 4H), 1.24 (t, $^3J = 7.1$ Hz, 6H), 1.23 (t, $^3J = 7.1$ Hz, 6H). $^{13}\text{C}\{^1\text{H}\}$ NMR (126 MHz, CDCl_3) δ 163.8, 154.7, 149.3, 147.2, 147.1, 140.3, 133.1, 132.3, 130.9, 130.5, 127.7, 127.5, 125.4, 125.0, 124.6, 122.5, 119.3, 112.2, 111.5, 110.9, 110.8, 44.6, 44.5, 12.8, 12.8. HRMS (ESI-TOF) m/z : $[\text{M}+\text{H}]$ Calcd for $\text{C}_{33}\text{H}_{36}\text{N}_3\text{O}_2$ 506.2802; Found 506.2774.

Suzuki-Miyaura cross-coupling reaction conditions on 3,5-dihalogenosalicylaldehyde: In a Schlenk tube, 3,5-dihalogenosalicylaldehyde (1 mmol.), 4-pyridinyl boronic acid (3 mmol.), base (3 mmol.) were dissolved in solvent (45 mL/mmol.). The resulting suspension was degassed with Argon before catalyst (5% mol.) was added. After a given time of stirring at a given temperature, using an oil bath, crude product was analyzed by ^1H NMR and purification on silica column chromatography eluting with $\text{CHCl}_3/\text{EtOH}$ (99:1) was performed, when the presence of expected coupling product was detected.

Optimized synthesis of salicylaldehyde 9: In a Schlenk tube, 3,5-dibromosalicylaldehyde (1 mmol.), 4-pyridinyl boronic acid (3 mmol.) and potassium carbonate (3 mmol.) were dissolved in 15 mL of toluene/ethanol 2/1. The resulting suspension was degassed with argon before $\text{PdCl}_2(\text{PPh}_3)$ (5% mol.) was added. Stirring was continued at 95°C using an oil bath for 15 hours before the crude solution was evaporated, taken up in dichloromethane and washed with water three times. Purification by chromatography on silica gel eluting with $\text{CHCl}_3/\text{EtOH}$ (99:1) afforded salicylaldehyde **9** as a yellow powder (171 mg, 62%). ^1H NMR (500 MHz, ^6d -DMSO) δ 11.57 (br, 1H), 10.21 (s, 1H), 8.70 – 8.68 (m, 2H), 8.67 – 8.65 (m, 2H), 8.40 (d, $^4J = 2.4$ Hz, 1H), 8.20 (d, $^4J = 2.4$ Hz, 1H), 7.88 – 7.84 (m, 2H), 7.77 – 7.72 (m, 2H). $^{13}\text{C}\{^1\text{H}\}$ NMR (126 MHz, ^6d -DMSO) δ 197.1, 158.4, 150.3, 149.6, 145.2, 143.5, 135.3, 132.6, 129.1, 127.8, 124.1, 122.1, 120.8. HRMS (ESI-TOF) m/z : $[\text{M}+\text{H}]$ Calcd for $\text{C}_{17}\text{H}_{13}\text{N}_2\text{O}_2$ 277.0972; Found 277.0964.

3,5-bromo-2-(2'-hydroxyphenyl)-5-tertiobutylbenzoxazole: To a solution of 4-tertiobutyl-2-aminophenol (0.5 mmol) in absolute ethanol (30 mL) was added 3,5-dibromo-2-

hydroxybenzaldehyde (0.5 mmol) and the resulting suspension was refluxed for 3 hours, using an oil bath. After cooling down, the solution was evaporated and redissolved in dichloromethane (50 mL), before 2,3-dichloro-5,6-dicyano-1,4-benzoquinone (DDQ) (0.6 mmol) dissolved in 100 mL dichloromethane was added dropwise. The resulting solution was stirred at room temperature overnight. After solvent evaporation, the crude residue was purified by silica gel chromatography eluting with Pet. Ether / CH₂Cl₂ 2:1 leading to 3,5-bromo-2-(2'-hydroxyphenyl)-5-tertbutylbenzoxazole as a white powder (204 mg, 96%). ¹H NMR (500 MHz, CDCl₃) δ 12.28 (s, 1H), 8.10 (d, ³J = 2.3 Hz, 1H), 7.78 (d, ⁴J = 2.3 Hz, 1H), 7.75 (d, ³J = 1.8 Hz, 1H), 7.53 (d, ³J = 8.7 Hz, 1H), 7.49 (dd, ³J = 8.7 Hz, ⁴J = 1.8 Hz, 1H), 1.41 (s, 9H). ¹³C{¹H} NMR (126 MHz, CDCl₃) δ 160.9, 154.5, 149.3, 147.3, 139.4, 138.5, 128.6, 124.2, 116.1, 112.9, 112.2, 111.2, 110.1, 35.12, 31.1. HRMS (ESI-TOF) m/z: [M+H] Calcd for C₁₇H₁₆Br₂NO₂ 425.9502; Found 425.9523.

Synthesis of 10 and 11: In a Schlenck tube, 3-bromosalicylaldehyde or 3,5-dibromosalicylaldehyde (1 mmol.), 4-pyridinyl boronic acid (1.5 or 3 mmol.) and potassium carbonate (1.5 or 3 mmol.) were dissolved in 15 mL of toluene/ethanol 2/1. The resulting suspension was degassed with argon before PdCl₂(PPh₃) (5% mol.) was added. Stirring was continued at 95°C using an oil bath for 15 hours before the crude solution was evaporated, taken up in dichloromethane and washed with water three times. Purification by chromatography on silica gel eluting with CH₂Cl₂ / Ethanol (98:2). afforded **10** and **11** as yellow solids.

10. Yellow solid (245 mg, 85%). ¹H NMR (500 MHz, CDCl₃) δ 12.19 (s, 1H), 8.70 (dd, ³J = 6.2 Hz, ⁴J = 1.7 Hz, 2H), 8.14 (dd, ³J = 7.9 Hz, ⁴J = 1.7 Hz, 1H), 7.77 – 7.72 (m, 1H), 7.67 (dd, ³J = 6.2 Hz, ⁴J = 1.7 Hz, 2H), 7.65 – 7.63 (m, 1H), 7.56 (dd, ³J = 7.6 Hz, ⁴J = 1.7 Hz, 1H), 7.45 – 7.39 (m, 2H), 7.14 (t, ³J = 7.8 Hz, 1H). ¹³C{¹H} NMR (126 MHz, CDCl₃) δ 162.9, 156.2, 149.5, 149.3, 145.9, 139.9, 134.2, 128.1, 127.2, 125.9, 125.4, 124.4, 120.0, 119.5, 111.5, 110.9. HRMS (ESI-TOF) m/z: [M+H] Calcd for C₁₈H₁₃N₂O₂ 289.0971, Found 289.0979.

11. Yellow solid (190 mg, 45%). ¹H NMR (500 MHz, CDCl₃) δ 12.40 (s, 1H), 8.80 – 8.68 (m, 4H), 8.39 (d, ⁴J = 2.4 Hz, 1H), 7.79 (d, ⁴J = 2.4 Hz, 1H), 7.76 (d, ⁴J = 1.9 Hz, 1H), 7.67 (d, ³J = 4.9 Hz, 2H), 7.62 – 7.56 (m, 3H), 7.51 (dd, ³J = 8.7 Hz, ⁴J = 1.9 Hz, 1H), 1.42 (s, 9H). ¹³C{¹H} NMR (126 MHz, CDCl₃) δ 162.4, 156.8, 150.6, 150.0, 149.4, 147.3, 146.8, 145.0, 139.6, 132.3, 129.9, 128.3, 126.1, 124.3, 124.1, 121.2, 116.1, 112.3, 110.1, 35.2, 31.9. HRMS (ESI-TOF) m/z: [M+H] Calcd for C₂₇H₂₄N₃O₂ 422.1863; Found 422.1854.

Synthesis of 12 and 13. MeI or BuI (1.1 mmol.) were added dropwise to a suspension of **10** (1 mmol.) in acetone (0.06 mol.L⁻¹). The resulting suspension was heated 4 hours at 60 °C using an oil bath for **12** or 48h for **13**. The mixture was concentrated *in vacuo* before the precipitate was filtered and washed with acetone and ethyl acetate.

12. Yellow solid. (258 mg, 60%). ¹H NMR (500 MHz, MeOD) δ 8.86 (d, *J* = 7.0 Hz, 2H), 8.76 (d, ⁴*J* = 2.4 Hz, 1H), 8.46 (d, ³*J* = 7.0 Hz, 2H), 8.18 (dd, ³*J* = 8.8 Hz, ⁴*J* = 2.5 Hz, 1H), 7.87 – 7.82 (m, 1H), 7.80 – 7.77 (m, 1H), 7.55 – 7.47 (m, 2H), 7.36 (d, ³*J* = 8.8 Hz, 1H), 4.39 (s, 3H). ¹³C{¹H} NMR (126 MHz, MeOD) δ 163.1, 163.1, 156.2, 150.7, 146.6, 141.0, 134.2, 128.7, 127.5, 126.8, 126.7, 124.9, 120.6, 120.1, 113.1, 112.0, 47.9. HRMS (ESI-TOF) *m/z*: [M+H] Calcd for C₁₉H₁₅N₂O₂ 303.1128; Found 303.1144.

13. Yellow solid (345 mg, 73%). ¹H NMR (500 MHz, MeOD) δ 8.95 (d, ³*J* = 7.0 Hz, 2H), 8.74 (d, ⁴*J* = 2.5 Hz, 1H), 8.46 (d, ³*J* = 7.0 Hz, 2H), 8.17 (dd, ³*J* = 8.8 Hz, ⁴*J* = 2.5 Hz, 1H), 7.85 – 7.80 (m, 1H), 7.78 – 7.76 (m, 1H), 7.55 – 7.46 (m, 2H), 7.33 (d, ³*J* = 8.8 Hz, 1H), 4.62 (t, ³*J* = 7.6 Hz, 2H), 2.10 – 1.99 (m, 2H), 1.57 – 1.42 (m, 2H), 1.05 (t, ³*J* = 7.4 Hz, 3H). ¹³C{¹H} NMR (126 MHz, MeOD) δ 163.2, 163.1, 156.4, 150.7, 145.6, 141.0, 134.3, 128.8, 127.5, 126.7, 126.5, 125.2, 120.6, 120.1, 113.1, 112.0, 61.8, 34.3, 20.5, 13.8. HRMS (ESI-TOF) *m/z*: [M+H] Calcd for C₂₂H₂₁N₂O₂ 345.1597, Found 345.1583.

14. **8** (1 mmol.) and 1-Chloro-2,4-dinitrobenzene (1.1 mmol.) were stirred in 50 mL of acetone at 60°C for 90 hours, using an oil bath. After cooling down, the precipitate was collected and washed three times with acetone and diethylether to yield **14**, as a yellow powder (299 mg, 61%). ¹H NMR (500 MHz, MeOD) δ 9.30 (d, ⁴*J* = 2.5 Hz, 1H), 9.22 – 9.17 (m, 2H), 8.94 (dd, ³*J* = 8.5 Hz, ⁴*J* = 2.5 Hz, 2H), 8.79 – 8.73 (m, 2H), 8.36 (dd, ³*J* = 8.9 Hz, ⁴*J* = 2.5 Hz, 1H), 8.33 (d, ³*J* = 8.7 Hz, 1H), 7.88 – 7.84 (m, 1H), 7.82 – 7.78 (m, 1H), 7.57 – 7.49 (m, 2H), 7.43 (d, ³*J* = 8.9 Hz, 1H). ¹³C{¹H} NMR (126 MHz, MeOD) δ 164.1, 163.0, 159.2, 151.1, 150.8, 146.6, 144.9, 141.0, 140.1, 134.9, 132.7, 131.1, 129.7, 127.6, 126.8, 126.1, 124.7, 123.3, 120.7, 120.4, 113.5, 112.1. HRMS (ESI-TOF) *m/z*: [M+H] Calcd for C₂₄H₁₅N₄O₆ 455.0986; Found 455.0977.

Synthesis of 15 and 16. **14** (1 mmol.) was dissolved in 30 mL of absolute ethanol before *p*-toluidine or 4-diethylamino-aniline (1.1 mmol.) were added. The resulting suspension was then heated at 80°C using an oil bath, for 60 hours. After cooling down, the precipitate was collected and washed with ethanol and diethylether several times.

15. Yellow solid. (241 mg, 58%). ¹H NMR (500 MHz, MeOD) δ 9.14 (d, ³*J* = 7.1 Hz, 2H), 8.83 (d, ⁴*J* = 2.5 Hz, 1H), 8.60 (d, ³*J* = 7.1 Hz, 2H), 8.26 (dd, ³*J* = 8.8 Hz, ⁴*J* = 2.5 Hz, 1H), 7.86 – 7.82 (m, 1H), 7.80 – 7.77 (m, 1H), 7.74 (d, ³*J* = 8.4 Hz, 2H), 7.58 (d, ³*J* = 7.9 Hz, 2H),

7.54 – 7.47 (m, 2H), 7.38 (d, $^3J = 8.8$ Hz, 1H), 2.53 (s, 3H). $^{13}\text{C}\{^1\text{H}\}$ NMR (126 MHz, MeOD) δ 163.5, 163.0, 157.0, 150.7, 145.4, 143.6, 141.7, 141.0, 134.5, 132.2, 129.0, 127.6, 126.8, 126.4, 125.0, 125.0, 120.6, 120.2, 113.3, 112.0, 21.2. HRMS (ESI-TOF) m/z : [M+H] Calcd for $\text{C}_{25}\text{H}_{19}\text{N}_2\text{O}_2$ 379.1441, Found 379.1427.

16. Dark red solid (109 mg, 48%). ^1H NMR (500 MHz, MeOD) δ 9.03 (br, 2H), 8.81 (s, 1H), 8.50 (br, 2H), 8.22 (d, $^3J = 8.7$ Hz, 1H), 7.85 (d, $^3J = 7.2$ Hz, 1H), 7.78 (d, $^3J = 7.3$ Hz, 1H), 7.61 (d, $^3J = 8.5$ Hz, 2H), 7.51 (q, $^3J = 7.6$ Hz, 2H), 7.36 (d, $^3J = 8.6$ Hz, 1H), 6.94 (d, $^3J = 8.4$ Hz, 2H), 3.52 (q, $^3J = 7.0$ Hz, 4H), 1.23 (t, $^3J = 7.1$ Hz, 6H). $^{13}\text{C}\{^1\text{H}\}$ NMR (126 MHz, MeOD) δ 155.4, 151.0, 144.4, 134.3, 131.7, 127.5, 126.7, 125.7, 124.8, 120.6, 113.2, 111.0, 45.6, 12.6. HRMS (ESI-TOF) m/z : [M+H] Calcd for $\text{C}_{28}\text{H}_{26}\text{N}_3\text{O}_2$ 436.2019; Found 436.2008.

Supporting Information. (^1H and ^{13}C NMR spectra, spectroscopic and details of the computational procedures and methods).

Acknowledgments

The authors thank the CNRS and the ANR for support in the framework of the GeDeMi grant (PhD fellowship for T.P.). C.D., A.D.L. and D.J. thank the CCIPL (*Centre de Calcul Intensif des Pays de la Loire*) installed in Nantes for generous allocation of computational time. T.S. acknowledges the ministère de l'enseignement supérieur, de la recherche et de l'innovation for a PhD fellowship.

References

- (1) (a) de Moliner, F.; Kielland, N.; Lavilla, R.; Vendrell, M. Modern Synthetic Avenues for the Preparation of Functional Fluorophores. *Angew. Chem., Int. Ed.*, **2017**, 56, 3758-3769. (b) Gao, M.; Yu, F.; Lv, C.; Choo, J.; Chen, L. Fluorescent chemical probes for accurate tumor diagnosis and targeting therapy. *Chem. Soc. Rev.*, **2017**, 46, 2237-2271. (c) Levi, L.; Muller, T. J. J. Multicomponent syntheses of functional chromophores. *Chem. Soc. Rev.*, **2016**, 45, 2825-2846.
- (2) (a) Chen, C.-L.; Chen, Y.-T.; Demchenko, A.P.; Chou, P.-T. Amino proton donors in excited-state intramolecular proton-transfer reactions. *Nat. Rev. Chem.*, **2018**, 2, 7, 131-143. (b) Massue, J.; Jacquemin, D.; Ulrich, G. Molecular Engineering of Excited-state Intramolecular Proton Transfer (ESIPT) Dual and Triple Emitters. *Chem. Lett.*, **2018**, 47, 9, 1083-1089. (c) Zhao, J.; Ji, S.; Chen, Y.; Guo, H.; Yang, P. Excited state intramolecular proton transfer (ESIPT): from principal photophysics to the development of new chromophores and applications in fluorescent molecular probes and luminescent materials. *Phys. Chem. Chem. Phys.* **2012**, 14, 8803-8817. (d) Mishra, V.R.; Ghanavatkar,

C.W.; Sekar, N. Towards NIR-Active Hydroxybenzazole (HBX)-Based ESIPT Motifs: A Recent Research Trend. *ChemSelect*, **2020**, 5, 2103-2113. (e) Padalkar, V.S.; Seki, S. Excited-state intramolecular proton-transfer (ESIPT)-inspired solid state emitters. *Chem. Soc. Rev.* **2016**, 45, 169-202. (f) Li, Y.; Dahal, D.; Abeywickrama, C.S.; Pang, Y. Progress in Tuning Emission of the Excited-State Intramolecular Proton Transfer (ESIPT)-Based Fluorescent Probes. *ACS Omega*, **2021**, 6, 6547-6553. (g) Berbigier, F.G.; Duarte, L.G.T.A.; Fialho Zawacki, M.; de Araújo, B.B.; de Moura Santos, C.; Atvars, T.D.Z.; Gonçalves, P.F.B.; Petzhold, C.L.; Rodembusch, F.S. ATRP Initiators Based on Proton Transfer Benzazole Dyes: Solid-State Photoactive Polymer with Very Large Stokes Shift. *ACS Appl. Polym. Mater.*, **2020**, 2, 1406-1416. (h) Berbigier, F.G.; Duarte, L.G.T.A.; Mendez Perez, J.; Araujo Mendes, R.; Zapp, E.; Atvars, T.D.Z.; Gonçalves Dal-Bó, A.; Rodembusch, F.S. Excited state intramolecular proton transfer process in benzazole fluorophores tailored by polymeric matrix: A combined theoretical and experimental study. *J. Mol. Liq.* **2019**, 295, 111710.

(3) (a) Raoui, M.; Massue, J.; Azarias, C.; Jacquemin, D.; Ulrich, G. Highly fluorescent extended 2-(2'-hydroxyphenyl)benzazole dyes: synthesis, optical properties and first-principle calculations. *Chem. Commun.* **2016**, 52, 9216-9219. (b) Heyer, E.; Benelhadj, K.; Budzák, S.; Jacquemin, D.; Massue, J.; Ulrich, G. On the Fine-Tuning of the Excited-State Intramolecular Proton Transfer (ESIPT) Process in 2-(2'-Hydroxybenzofuran)benzazole (HBBX) Dyes. *Chem. Eur. J.* **2017**, 23, 7324-7336. (c) Ren, Y.; Fan, D.; Ying H.; Li, X. Rational design of the benzothiazole-based fluorescent scaffold for tunable emission. *Tetrahedron Lett.*, **2019**, 60, 1060-1065.

(4) Zhang, M.; Cheng, R.; Lan, J.; Zhang, H.; Yan, L.; Pu, X.; Huang, Z.; Wu, D.; You, J. Oxidative C-H/C-H Cross-Coupling of [1,2,4]Triazolo[1,5- a]pyrimidines with Indoles and Pyrroles: Discovering Excited-State Intramolecular Proton Transfer (ESIPT) Fluorophores. *Org. Lett.*, **2019**, 21, 4058-4062.

(5) Tseng, H.-W.; Lin, T.-C.; Chen, C.-L.; Lin, T.-C.; Chen, Y.-A.; Liu, J.-Q.; Hung, C.-H.; Chao, C.-M.; Liu, K.-M.; Chou, P.-T. A new class of N-H proton transfer molecules: wide tautomer emission tuning from 590 nm to 770 nm via a facile, single site amino derivatization in 10-aminobenzo[h]quinolone. *Chem. Commun.*, **2015**, 51, 16099-16102.

(6) (a) Liu, H.; Cheng, X.; Zhang, H.; Wang, Y.; Zhang, H.; Yamaguchi, S. ESIPT-active organic compounds with white luminescence based on crystallization-induced keto emission (CIKE). *Chem. Commun.*, **2017**, 53, 7832-7835. (b) Mutai, T.; Muramatsu, T.; Yoshikawa, I.; Houjou, H.; Ogura, M. Development of Imidazo[1,2-a]pyridine Derivatives with an Intramolecular Hydrogen-Bonded Seven-Membered Ring Exhibiting Bright ESIPT Luminescence in the Solid State. *Org. Lett.*, **2019**, 21, 2143-2146. (c) Gobel, D.; Duvinage, D.; Stauch, T.; Nachtsheim, B.J. Nitrile-substituted 2-(oxazolonyl)-phenols: minimalistic excited-state intramolecular proton transfer (ESIPT)-based fluorophores. *J. Mater. Chem. C*, **2020**, 8, 9213-9225.

(7) (a) Wei, Y.C.; Zhang, Z.; Chen, Y.-A.; Wu, C.-H.; Liu, Z.-Y.; Ho, S.-Y.; Liu, J.-C.; Lin, J.-A.; Chou, P.-T. Mechanochromism induced through the interplay between excimer reaction and excited

state intramolecular proton transfer. *Nat. Chem. Commun.*, **2019**, 2, 1, 1-9. (b) Horak, E.; Robic, M.; Simanovic, A.; Mandic, V.; Vianello, R.; Hranjec, M.; Murkovic Steinberg, I. Tuneable solid-state emitters based on benzimidazole derivatives: Aggregation induced red emission and mechanochromism of D- π -A fluorophores. *Dyes Pigm.*, **2019**, 162, 688-696.

(8) (a) Biswas, S.; Mengji, R.; Barman, S.; Venugopal, V.; Jana, A.; Singh, N.D.P. 'AIE + ESIPT' assisted photorelease: fluorescent organic nanoparticles for dual anticancer drug delivery with real-time monitoring ability. *Chem. Commun.*, **2018**, 54, 168-171. (b) Feng, Q.; Li, Y.; Wang, L.; Li, C.; Wang, J.; Liu, Y.; Li, K.; Hou, H. Multiple-color aggregation-induced emission (AIE) molecules as chemodosimeters for pH sensing. *Chem. Commun.*, **2016**, 52, 3123-3126. (c) Li, K.; Feng, Q.; Niu, G.; Zhang, W.; Li, Y.; Kang, M.; Xu, K.; He, J.; Hou, H.; Tang, B.Z. Benzothiazole-Based AIEgen with Tunable Excited-State Intramolecular Proton Transfer and Restricted Intramolecular Rotation Processes for Highly Sensitive Physiological pH Sensing. *ACS Sens.*, **2018**, 3, 920-928. (d) Dwivedi, B.K.; Singh, V.D.; Paitandi, R.P.D.; Pandey, S. Substituent-directed ESIPT-coupled Aggregation-induced Emission in Near-infrared-emitting Quinazoline Derivatives. *ChemPhysChem.*, **2018**, 19, 2672-2682.

(9) (a) Sedgwick, A.C.; Wu, L.; Han, H.-H.; Bull, S.D.; He, X.-P.; James, T.D.; Sessler, J.L.; Tang, B.Z.; Tian, H.; Yoon, J. Excited-state intramolecular proton-transfer (ESIPT) based fluorescence sensors and imaging agents. *Chem. Soc. Rev.*, **2018**, 47, 8842-8880. (b) Saravana Kumar, P.; Raja Lakshmi, P.; Elango, K.P. An easy to make chemoreceptor for the selective ratiometric fluorescent detection of cyanide in aqueous solution and in food material. *New J. Chem.*, **2019**, 43, 675-680. (c) Sinha, S.; Chowdhury, B.; Ghosh, P. A Highly Sensitive ESIPT-Based Ratiometric Fluorescence Sensor for Selective Detection of Al³⁺. *Inorg. Chem.*, **2016**, 55, 9212-9220.

(10) (a) Benelhadj, K.; Muzuzu, W.; Massue, J.; Retailleau, P.; Charaf-Eddin, A.; Laurent, A.D.; Jacquemin, D.; Ulrich, G.; Ziessel, R. White Emitters by Tuning the Excited-State Intramolecular Proton-Transfer Fluorescence Emission in 2-(2'-Hydroxybenzofuran)benzoxazole Dyes. *Chem. Eur. J.*, **2014**, 20, 12843-12857. (b) Li, B.; Lan, J.; Wu, D.; You, J. Rhodium(III)-Catalyzed ortho-Heteroarylation of Phenols through Internal Oxidative C-H Activation: Rapid Screening of Single-Molecular White-Light-Emitting Materials. *Angew. Chem., Int. Ed.*, **2015**, 54, 14008-14012. (c) Park, S.; Kwon, J.E.; Kim, S.H.; Seo, J.; Chung, K.; Park, S.-Y.; Jang, D.-J.; Medina, B.M.; Gierschner, J.; Park, S.Y. A White-Light-Emitting Molecule: Frustrated Energy Transfer between Constituent Emitting Centers. *J. Am. Chem. Soc.* **2009**, 131, 14043-14049. (d) Tang, K.-C.; Chang, M.-J.; Lin, T.-Y.; Pan, H.-A.; Fang, T.-C.; Chen, K.-Y.; Hung, W.-Y.; Hsu, Y.-H.; Chou, P.-T. Fine Tuning the Energetics of Excited-State Intramolecular Proton Transfer (ESIPT): White Light Generation in a Single ESIPT System. *J. Am. Chem. Soc.* **2011**, 133, 17738-17745. (e) Duarte, L.G.T.A.; Germino, J.C.; Mendes, R.A.; Berbigier, J.F.; Faleirosa, M.M.; Rodembusch, F.S.; Atvars, T.D.Z. The role of a simple and effective salicylidene derivative. Spectral broadening and performance improvement of PFO-based all-solution processed OLEDs. *Dyes Pigm.*, **2019**, 171, 107671. (f) Duarte, L.G.T.A.;

- Germino, J.C.; Berbigier, J.F.; Barboza, C.A.; Faleiros, M.M.; de Alencar Simoni, D.; Galante, M.T.; de Holanda, M.S.; Rodembusch, F.S.; Atvars, T.D.Z. White-light generation from all-solution-processed OLEDs using a benzothiazole-salophen derivative reactive to the ESIPT process. *Phys. Chem., Chem. Phys.*, **2019**, *21*, 1172-1182.
- (11) Zhang, Y.; Yang, H.; Ma, H.; Bian, G.; Zang, Q.; Sun, J.; Zhang, C.; An, Z.; Wang, W.-Y. Excitation Wavelength Dependent Fluorescence of an ESIPT Triazole Derivative for Amine Sensing and Anti-Counterfeiting Applications. *Angew. Chem., Int. Ed.*, **2019**, *58*, 8773-8778.
- (12) (a) Raghuvanshi, A.; Jha, A.K.; Sharma, A.; Umar, S.; Mishra, S.; Kant, R.; Goel, A. A Nonarchetypal 5,6-Dihydro-2H-pyrano[3,2-g]indolizine-Based Solution-Solid Dual Emissive AIEgen with Multicolor Tunability. *Chem. Eur. J.* **2017**, *23*, 4527-4531. (b) Qiu, Q.; Xu, P.; Zhu, Y.; Yu, J.; Wei, M.; Xi, W.; Feng, H.; Chen, J.; Qian, Z. Rational Design of Dual-State Emission Luminogens with Solvatochromism by Combining a Partially Shared Donor–Acceptor Pattern and Twisted Structures. *Chem. Eur. J.* **2019**, *25*, 15983-15987. (c) Stoerkler, T.; Frath, D.; Jacquemin, D.; Massue, J.; Ulrich, G. Dual-State Emissive π -Extended Salicylaldehyde Fluorophores: Synthesis, Photophysical Properties and First-Principle Calculations. *Eur. J. Org. Chem.*, **2021**, *26*, 3726-3736.
- (13) (a) Takagi, K.; Ito, K.; Yamada, Y.; Nakashima, T.; Fukuda, R.; Ehara, M.; Masu, H. Synthesis and Optical Properties of Excited-State Intramolecular Proton Transfer Active π -Conjugated Benzimidazole Compounds: Influence of Structural Rigidification by Ring Fusion. *J. Org. Chem.* **2017**, *82*, 12173-12180. (b) Pariat, T.; Munch, M.; Durko-Maciag, M.; Mysliwicz, J.; Retailleau, P.; Vérité, P. M.; Jacquemin, D.; Massue, J.; Ulrich, G. Impact of Heteroatom Substitution on Dual-State Emissive Rigidified 2-(2'-hydroxyphenyl)benzazole Dyes: Towards Ultra-Bright ESIPT Fluorophores. *Chem. Eur. J.*, **2021**, *27*, 10, 3483-3495.
- (14) Skonieczny, K.; Yoo, J.; Larsen, J.M.; Espinoza, E.M.; Barbasiewicz, M.; Vullev, V.I.; Lee, C.-H.; Gryko, D.-T. How To Reach Intense Luminescence for Compounds Capable of Excited-State Intramolecular Proton Transfer? *Chem. Eur. J.* **2016**, *22*, 7485-7496.
- (15) Suzuki, N.; Suda, K.; Yokogawa, D.; Kitoh-Nishioka, H.; Irlé, S.; Ando, A.; Abegão, L.M.G.; Kamada, K.; Fukazawa, A.; Yamaguchi, S. Near infrared two-photon-excited and -emissive dyes based on a strapped excited-state intramolecular proton-transfer (ESIPT) scaffold. *Chem. Sci.*, **2018**, *9*, 2666-2673.
- (16) (a) Massue, J.; Felouat, A.; Curtil, M.; Vérité, P.M.; Jacquemin, D.; Ulrich, G. Solution and solid-state Excited-State Intramolecular Proton Transfer (ESIPT) emitters incorporating Bis-triethyl- or triphenylsilylethynyl units. *Dyes Pigm.*, **2019**, *160*, 915-922. (b) Massue, J.; Ulrich, G.; Ziesel, R. Effect of 3,5-Disubstitution on the Optical Properties of Luminescent 2-(2'-Hydroxyphenyl)benzoxazoles and Their Borate Complexes. *Eur. J. Org. Chem.*, **2013**, 5701-5709.
- (17) Massue, J.; Pariat, T.; Vérité, P. M.; Jacquemin, D.; Durko, M.; Chtouki, T.; Sznitko, L.; Mysliwicz, J.; Ulrich, G. Natural Born Laser Dyes: Excited-State Intramolecular Proton Transfer (ESIPT) Emitters and Their Use in Random Lasing Studies. *Nanomaterials*, **2019**, *9*, 1093.

- (18) Munch, M.; Curtil, M.; Vérité, P.M.; Jacquemin, D.; Massue, J.; Ulrich, G. Ethynyl-Tolyl Extended 2-(2'-Hydroxyphenyl)benzoxazole Dyes: Solution and Solid-state Excited-State Intramolecular Proton Transfer (ESIPT) Emitters. *Eur. J. Org. Chem.*, **2019**, 1134-1144.
- (19) Azarias, C.; Budzak, S.; Laurent, A. D.; Ulrich, G.; Jacquemin, D. Tuning ESIPT fluorophores into dual emitters. *Chem. Sci.* **2016**, *7*, 3763–3774.
- (20) Hossen, T.; Sahu, K. Photo-induced Electron Transfer or Proton-Coupled Electron Transfer in Methylbipyridine/Phenol Complexes: A Time-Dependent Density Functional Theory Investigation. *J. Phys. Chem. A*, **2019**, *123*, 8122-8129.
- (21) (a) Huang, Y.; You, X.; Wang, L.; Zhang, G.; Gui, S.; Jin, Y.; Zhao, R.; Zhang, D. Pyridinium-Substituted Tetraphenylethylenes Functionalized with Alkyl Chains as Autophagy Modulators for Cancer Therapy. *Angew. Chem., Int. Ed.*, **2020**, *59*, 10042-10051. (b) Kang, H.; Facchetti, A.; Jiang, H.; Cariati, E.; Righetto, S.; Ugo, R.; Zuccaccia, C.; Macchioni, A.; Stern, C.L.; Liu, Z.; Ho, S.-T.; Brown, E.C.; Ratner, M.A.; Marks, T.J. Ultralarge Hyperpolarizability Twisted π -Electron System Electro-Optic Chromophores: Synthesis, Solid-State and Solution-Phase Structural Characteristics, Electronic Structures, Linear and Nonlinear Optical Properties, and Computational Studies. *J. Am. Chem. Soc.*, **2007**, *129*, 3267-3286.
- (22) (a) Chen, Y.; Fang, Y.; Gu, H.; Qiang, J.; Li, H.; Fan, J.; Cao, J.; Wang, F.; Lu, S.; Chen, X. Color-Tunable and ESIPT-Inspired Solid Fluorophores Based on Benzothiazole Derivatives: Aggregation-Induced Emission, Strong Solvatochromic Effect, and White Light Emission. *ACS Appl. Mater. Interfaces*, **2020**, *12*, 55094-55106. (b) Abeywickrama, C.S.; Pang, Y. Synthesis of a bis[2-(2'-hydroxyphenyl)benzoxazole]pyridinium derivative: the fluoride-induced large spectral shift for ratiometric response. *New J. Chem.*, **2021**, *45*, 9102-9108.
- (23) Ren, H.; Huo, F.; Wu, X.; Liu, X.; Yin, C. An ESIPT-induced NIR fluorescent probe to visualize mitochondrial sulfur dioxide during oxidative stress in vivo. *Chem. Commun.*, **2021**, *57*, 655-658.
- (24) Olesinska, M.; Wu, G.; Gomez-Coca, S.; Anton-Garcia, D.; Szabo, I.; Rosta, E.; Scherman, O. A. Modular supramolecular dimerization of optically tunable extended aryl viologens. *Chem. Sci.*, **2019**, *10*, 8806-8811.